ELSEVIER

Journal of Fluids and Structures 19 (2004) 957–984

JOURNAL OF FLUIDS AND STRUCTURES

www.elsevier.nl/locate/jnlabr/yjfls

Influence of a rigid coaxial core on the stress–strain state of a submerged fluid-filled circular cylindrical shell subjected to a shock wave

S. Iakovlev

Department of Engineering Mathematics, Dalhousie University, Halifax, Nova Scotia, Canada B3J 2X4

Accepted 31 May 2004

Abstract

A submerged fluid-filled circular cylindrical shell containing a rigid coaxial cylindrical core is considered. The nonstationary dynamics of such a system subjected to an external spherical shock wave is examined, with particular emphasis on the influence that a core has on the stress–strain state of the shell. A complete diffraction–radiation problem is considered, and an analytical–numerical solution of the problem is obtained. The influence of several different cores is analyzed, and a comparison to the case of a shell without a core is presented. Physical phenomena occurring in the shell and in the internal fluid are studied in detail. Two- and three-dimensional graphics is used to illustrate and analyze the nonstationary dynamics of the stress–strain state. The possibility of using a rigid core as a measure of constructive safety improvement is discussed.

1. Introduction

The study of the dynamics of a circular cylindrical shell structure filled with and submerged into fluid, and subjected to a hydrodynamic shock wave, is of considerable interest to naval architecture and ocean engineering. The primary goal here is the stress analysis of offshore structures and submersible marine vehicles experiencing underwater explosions. The topic appears to be of theoretical interest as well because of many challenges, both mathematical and experimental, that one faces studying this complex fluid–structure interaction process.

The present paper examines the dynamics of a submerged fluid-filled shell when an extra structural element, namely a rigid circular cylindrical structure of a smaller radius placed coaxially within the shell, is added to the system. The reason for undertaking rigorous study of this particular design is as follows. It has recently been shown (Iakovlev, 2002a) that wave phenomena play a determining role in the stress state of a submerged fluid-filled circular cylindrical shell. In particular, it was found that the maximum stress in the structure can be caused not only by the direct action of the incident shock wave or elastic waves propagating in the shell, but also by hydrodynamic waves propagating in the internal fluid. In the light of these results, it is reasonable to expect that, as long as the wave pattern in the internal fluid is changed, the stress state of the shell will change as well. Although it is not clear at this point if these changes will lead to significantly lower stresses, verification of this assumption is of considerable practical interest. If such a reduction of stresses does occur, a number of applications aiming at constructive safety improvement will easily follow.

E-mail address: serguei.iakovlev@dal.ca (S. Iakovlev).

0889-9746/$ - see front matter
doi:10.1016/j.jfluidstructs.2004.05.003

Nomenclature

a	radius of the core $\bar{a} = ar_0^{-1}$
b_{mn}	harmonic of the normal incident velocity $\bar{b}_{mn} = b_{mn}c_e^{-1}$
$\bar{B}_{mn}$	Laplace transform of $\bar{b}_{mn}$
c_e	sound speed in the external fluid $\bar{c}_e = 1$
c_i	sound speed in the internal fluid $\bar{c}_i = c_i c_e^{-1}$
c_s	sound speed in the shell material $\bar{c}_s = c_s c_e^{-1}$
c_{mn}^{ij}	coefficient of the integro-differential system for the displacement harmonics
D_{mn}	an arbitrary function
E	Young's modulus of the shell material $\bar{E} = E\rho_e^{-1}c_e^{-2}$
E_k	kinetic energy per unit area of the shell $\bar{E}_k = E_k\rho_e^{-1}c_e^{-2}r_0^{-3}$
E_p	strain energy per unit area of the shell $\bar{E}_p = E_p\rho_e^{-1}c_e^{-2}r_0^{-3}$
F_{mn}	an arbitrary function
G_{mn}	an arbitrary function
h_0	thickness of the shell $\bar{h}_0 = h_0 r_0^{-1}$
H	Heaviside unit step function
I_n	modified Bessel function of the first kind of order n
J_1	Bessel function of the first kind of order n
k_0	coefficient in the shell equations $\bar{k}_0 = k_0 r_0^{-1}$
K_n	modified Bessel function of the second kind of order n
L	axial dimension of the affected region of the shell/fluids $\bar{L} = Lr_0^{-1}$
m	a summation index
$\tilde{m}$	a temporary variable
n	a summation index
p	total hydrodynamic pressure on the shell surface $\bar{p} = p\rho_e^{-1}c_e^{-2}$
p_{mn}	harmonic of the total hydrodynamic pressure on the shell surface $\bar{p}_{mn} = p_{mn}\rho_e^{-1}c_e^{-2}$
p_0	incident pressure on the shell surface $\bar{p}_0 = p_0\rho_e^{-1}c_e^{-2}$
p_{mn}^0	harmonic of the incident pressure on the shell surface $\bar{p}_{mn}^0 = p_{mn}^0\rho_e^{-1}c_e^{-2}$
p_α	pressure in the front of the shock wave at the moment it reaches the shell $\bar{p}_\alpha = p_\alpha\rho_e^{-1}c_e^{-2}$
p_d	diffraction pressure on the shell surface $\bar{p}_d = p_d\rho_e^{-1}c_e^{-2}$
p_{mn}^d	harmonic of the diffraction pressure on the shell surface $\bar{p}_{mn}^d = p_{mn}^d\rho_e^{-1}c_e^{-2}$
p_e	total pressure in the external fluid $\bar{p}_e = p_e\rho_e^{-1}c_e^{-2}$
p_i	total pressure in the internal fluid $\bar{p}_i = p_i\rho_e^{-1}c_e^{-2}$
p_r^e	external radiation pressure on the shell surface $\bar{p}_r^e = p_r^e\rho_e^{-1}c_e^{-2}$
$p_{mn}^{r,e}$	harmonic of the external radiation pressure on the shell surface $\bar{p}_{mn}^{r,e} = p_{mn}^{r,e}\rho_e^{-1}c_e^{-2}$
p_r^i	internal radiation pressure on the shell surface $\bar{p}_r^i = p_r^i\rho_e^{-1}c_e^{-2}$
$p_{mn}^{r,i}$	harmonic of the internal radiation pressure on the shell surface $\bar{p}_{mn}^{r,i} = p_{mn}^{r,i}\rho_e^{-1}c_e^{-2}$
r	radial coordinate of the cylindrical coordinate system $\bar{r} = rr_0^{-1}$
r_0	radius of the middle surface of the shell $\bar{r}_0 = 1$
R	radial coordinate of the spherical coordinate system centered at the source of the shock wave $\bar{R} = Rr_0^{-1}$
R_0	distance between the source of the shock wave and the axis of the shell $\bar{R}_0 = R_0 r_0^{-1}$
R_1	distance between the source of the shock wave and a point on the shell surface $\bar{R}_1 = R_1 r_0^{-1}$
s	Laplace transform variable
S_R	shock wave source stand-off $\bar{S}_R = S_R r_0^{-1}$
t	time $\bar{t} = t\,c_e r_0^{-1}$
t_c^1	time of arrival of the first ('primary') core-reflected wave at the head point of the shell $\bar{t}_c^1 = t_c^1 c_e r_0^{-1}$
t_c^2	time of arrival of the second core-reflected wave at the head point of the shell $\bar{t}_c^2 = t_c^2 c_e r_0^{-1}$
u	longitudinal displacement of the middle surface of the shell $\bar{u} = ur_0^{-1}$
u_{mn}	harmonic of the longitudinal displacement $\bar{u}_{mn} = u_{mn}r_0^{-1}$

v	transverse displacement of the middle surface of the shell $\bar{v} = vr_0^{-1}$
v_{mn}	harmonic of the transverse displacement $\bar{v}_{mn} = v_{mn}r_0^{-1}$
w	normal displacement of the middle surface of the shell $\bar{w} = wr_0^{-1}$
$\bar{W}$	Laplace transform of $\bar{w}$
w_{mn}	harmonic of the normal displacement $\bar{w}_{mn} = w_{mn}r_0^{-1}$
$\bar{W}_{mn}$	Laplace transform of $\bar{w}_{mn}$
x	axial coordinate of the cylindrical coordinate system $\bar{x} = xr_0^{-1}$
β_m	a temporary variable
γ	reciprocal of the dimensionless sound speed in the shell material
Δ_{mn}	a temporary variable
ε_1	longitudinal strain in the middle surface of the shell $\bar{\varepsilon}_1 = \varepsilon_1$
ε_2	transverse strain in the middle surface of the shell $\bar{\varepsilon}_2 = \varepsilon_2$
θ	angular coordinate of the cylindrical coordinate system
κ_1	longitudinal change of curvature of the middle surface of the shell $\bar{\kappa}_1 = \kappa_1 r_0$
κ_2	transverse change of curvature of the middle surface of the shell $\bar{\kappa}_2 = \kappa_2 r_0$
λ	exponential decay constant $\bar{\lambda} = \lambda c_e r_0^{-1}$
ν	Poisson's ratio of the shell material
ξ	integration variable for convolution and convolution-like integrals
ρ_e	density of the exterior fluid $\bar{\rho}_e = 1$
ρ_i	density of the interior fluid $\bar{\rho}_i = \rho_i \rho_e^{-1}$
ρ_s	density of the shell material $\bar{\rho}_s = \rho_s \rho_e^{-1}$
σ_{11}	longitudinal stress $\bar{\sigma}_{11} = \sigma_{11}\rho_e^{-1}c_e^{-2}$
σ_{12}	shear stress $\bar{\sigma}_{12} = \sigma_{12}\rho_e^{-1}c_e^{-2}$
σ_{22}	transverse stress $\bar{\sigma}_{22} = \sigma_{22}\rho_e^{-1}c_e^{-2}$
σ_{11}^0	membrane component of the longitudinal stress $\bar{\sigma}_{11}^0 = \sigma_{11}^0\rho_e^{-1}c_e^{-2}$
σ_{12}^0	membrane component of the shear stress $\bar{\sigma}_{12}^0 = \sigma_{12}^0\rho_e^{-1}c_e^{-2}$
σ_{22}^0	membrane component of the transverse stress $\bar{\sigma}_{22}^0 = \sigma_{22}^0\rho_e^{-1}c_e^{-2}$
σ_{11}^b	bending component of the longitudinal stress $\bar{\sigma}_{11}^b = \sigma_{11}^b\rho_e^{-1}c_e^{-2}$
σ_{12}^b	bending component of the shear stress $\bar{\sigma}_{12}^b = \sigma_{12}^b\rho_e^{-1}c_e^{-2}$
σ_{22}^b	bending component of the transverse stress $\bar{\sigma}_{22}^b = \sigma_{22}^b\rho_e^{-1}c_e^{-2}$
τ	torsion of the middle surface of the shell $\bar{\tau} = \tau r_0$
ϕ	total fluid velocity potential $\bar{\phi} = \phi c_e^{-1} r_0^{-1}$
ϕ_0	fluid velocity potential in the incident wave $\bar{\phi}_0 = \phi_0 c_e^{-1} r_0^{-1}$
ϕ_d	fluid velocity potential in the diffracted wave $\bar{\phi}_d = \phi_d c_e^{-1} r_0^{-1}$
$\bar{\Phi}_d$	Laplace transform of $\bar{\phi}_d$
$\bar{\Phi}_{mn}^d$	harmonic of the Laplace transform of $\bar{\phi}_d$
ϕ_e	fluid velocity potential in the external fluid $\bar{\phi}_e = \phi_e c_e^{-1} r_0^{-1}$
$\bar{\Phi}_e$	Laplace transform of $\bar{\phi}_e$
$\bar{\Phi}_{mn}^e$	harmonic of the Laplace transform of $\bar{\phi}_e$
ϕ_i	fluid velocity potential in the internal fluid $\bar{\phi}_i = \phi_i c_e^{-1} r_0^{-1}$
$\bar{\Phi}_i$	Laplace transform of $\bar{\phi}_i$
$\bar{\Phi}_{mn}^i$	harmonic of the Laplace transform of $\bar{\phi}_i$
ϕ_r^e	fluid velocity potential in the external radiated wave $\bar{\phi}_r^e = \phi_r^e c_e^{-1} r_0^{-1}$
$\bar{\Phi}_r^e$	Laplace transform of $\bar{\phi}_r^e$
$\bar{\Phi}_{mn}^{r,e}$	harmonic of the Laplace transform of $\bar{\phi}_r^e$
ϕ_r^i	fluid velocity potential in the internal radiated wave $\bar{\phi}_r^i = \phi_r^i c_e^{-1} r_0^{-1}$
$\bar{\Phi}_r^i$	Laplace transform of $\bar{\phi}_r^i$
$\bar{\Phi}_{mn}^{r,i}$	harmonic of the Laplace transform of $\bar{\phi}_r^i$
χ	a temporary variable

ψ_n^e	two-dimensional 'exterior' response functions
ψ_n^i	two-dimensional 'interior' response functions
Ψ_n^e	Laplace transform of ψ_n^e
Ψ_n^i	Laplace transform of ψ_n^i
ψ_{mn}^e	three-dimensional 'exterior' response functions
ψ_{mn}^i	three-dimensional 'interior' response functions
Ψ_{mn}^e	Laplace transform of ψ_{mn}^e
Ψ_{mn}^i	Laplace transform of ψ_{mn}^i
Ω	shear strain in the middle surface of the shell $\bar{\Omega} = \Omega$

Since we are interested in practically feasible design ideas, the discussion can be narrowed down to a more specific question: is there any constructively reasonable way to eliminate (or at least reduce) the destructive influence of the wave effects in the internal fluid? In the present paper, a rigid coaxial core is proposed as a design advancement aiming to change the wave pattern in the internal fluid. Such an idea would be relatively easy to implement in engineering practice, should it be found that the stress reduction is substantial.

Structural dynamics of circular cylindrical shells subjected to hydrodynamic shock waves was first addressed in order to provide naval architects with information about the dynamic response of submersible vehicles to underwater explosions and acoustic pulses. An empty submerged shell was considered as a model [classical works by Mindlin and Bleich (1953) and Haywood (1958) can be mentioned here]. In the following three decades, submerged and/or fluid-filled shells were studied very extensively, and various types of incident shock loads were analyzed [e.g. Geers (1969), Huang and Wang (1970) and Carpenter and Berger (1972)]. However, it seems that the structural dynamics of a shell, especially three-dimensional stress–strain states, were not addressed consistently enough, partly because of the limited computational capabilities available at that time. The majority of the solutions proposed were either analytical or semianalytical, often involving numerical inversion of the Laplace, Hankel, or Fourier transforms, or their combinations, which imposed certain limitations on extensive simulations of the structural dynamics. A few more references to the work published in the 1950s–1970s can be found in Iakovlev (2002a).

Nowadays, much more consistent and detailed study of the fluid–structure interaction is being undertaken to analyze the nonstationary dynamics of cylindrical shells experiencing shock loads. The majority of publications employ various numerical techniques, and make use of both commercial codes and algorithms specifically developed for particular problems. For example, Wardlaw and Luton (2000) and Chambers et al. (2001) considered an explosion in a fluid-filled cylinder, while Aanhold et al. (1998) examined the interaction of a shock wave with a floating vessel. Doubly asymptotic approximations are also extensively employed to study fluid-filled and/or submerged structures [e.g., Geers and Zhang, 1994a,b]. Ofengeim and Drikakis (1997) and Drikakis et al. (1997) addressed the interaction between a shock wave and a rigid cylinder in the gas dynamics context. In general, it seems that quite often the authors tend to pay more attention to hydrodynamic aspects of the interaction, such as cavitation and gas bubble dynamics. In some works, the normal displacements and/or velocities of a structure are addressed, but this analysis is mostly related to the discussion of the hydrodynamic phenomena.

There are also numerous works studying acoustic phenomena associated with shell–fluid interaction. Recent publications do tend to address rather complex systems [e.g. a stiffened shell was considered by Baillard et al. (2000), and a finite shell with hemispherical endcaps was addressed by Touraine et al. (2000)]. Although these works have some common aspects with the problems discussed here, the difference is quite significant. Specifically, the interaction with shock waves is an essentially nonstationary process, and this is what makes the results obtained for acoustical problems of little use when it comes to geometrically similar structures but nonstationary loading.

Thus, it seems that the interaction between a circular cylindrical shell and a shock wave is quite well studied and understood. However, the stress–strain states of complex shell systems appear to be understudied, at least in the context of structural safety. The present paper offers such a study, focusing on the detailed analysis of the stress–strain state of a fluid-filled submerged elastic circular cylindrical shell with a rigid coaxial core when the system is experiencing a spherical hydrodynamic shock wave.

We should mention that from a constructive point of view, a slightly different idea may appear to be more feasible. Specifically, a 'secondary' circular cylindrical shell placed coaxially with the 'primary' one seems to be a more natural constructive advancement as opposed to the rigid core. Therefore, one may question the priority of the study presented here over the analysis of a two-shell system.

Certainly, dynamic analysis of a two-shell system is of considerable interest. However, the physics of the fluid–structure interaction is much more complicated in that case. Unlike a rigid core, the deformations of the inner shell will induce radiation pressures which will contribute to the total hydrodynamic field. As a result, the stress–strain state of the outer shell will change as well. Since in this case there are up to five media with different properties (the outer shell, the inner shell, the external fluid, the fluid in between the shells, and possibly the fluid inside the inner shell), it becomes extremely difficult to predict the dynamics of the stress–strain state relying only on 'engineering common sense'. A detailed study based on a three-dimensional mathematical model that incorporates all the media is needed.

It is quite apparent that such a model will be considerably more complex than the one addressed in this paper, even though the models would have a lot in common (very similar geometries, identical loading etc.). Therefore, aside from the practical and theoretical interest that a solid-core problem generates on its own, one can view the analysis presented here as the first step towards understanding the nonstationary dynamics of fluid-interacting shell systems that are significantly more structurally complex. The author intends to consider a two-shell problem in the foreseeable future.

2. Mathematical formulation

We consider a thin elastic circular cylindrical shell of radius r_0 and thickness h_0 filled with linearly compressible inviscid fluid and submerged into another such fluid. The density of and the sound speed in the internal and external fluids are ρ_i, c_i, and ρ_e, c_e, respectively. The material of the shell is isotropic, and is characterized by the density ρ_s, sound speed c_s, Young's modulus E, and Poisson's ratio ν. The thickness-to-radius ratio is assumed to be small enough so that thin-shell theory can be applied. The normal (radial), transverse (azimuthal), and longitudinal (axial) displacements of the middle surface of the shell are w, v, and u, respectively. A rigid circular cylinder of radius $a<r_0$ is placed coaxially within the shell. The system is subjected to a spherical shock wave with the source located at the distance R_0 from the axis of the shell. A cylindrical coordinate system based on the axis of the shell is considered. Fig. 1 shows the geometry of the problem.

The fluids are governed by the wave equations

$$\nabla^2\phi_e = \frac{1}{c_e^2}\frac{\partial^2\phi_e}{\partial t^2} \tag{1}$$

and

$$\nabla^2\phi_i = \frac{1}{c_i^2}\frac{\partial^2\phi_i}{\partial t^2}, \tag{2}$$

where ϕ_e and ϕ_i are the fluid velocity potentials in the external and internal fluids, respectively.

The hydrodynamic pressures in the external and internal fluids, p_e and p_i, respectively, are

$$p_e = -\rho_e\frac{\partial\phi_e}{\partial t} \quad \text{and} \quad p_i = -\rho_i\frac{\partial\phi_i}{\partial t}. \tag{3}$$

The strain energy per unit area of the shell E_p is given by (Love, 1927)

$$E_p = \frac{Eh_0}{2(1-\nu^2)}\left\{\varepsilon_1^2+\varepsilon_2^2+2\nu\varepsilon_1\varepsilon_2+\frac{1}{2}(1-\nu)\Omega^2+k_0^2(\kappa_1^2+\kappa_2^2+2\nu\kappa_1\kappa_2+2(1-\nu)\tau^2)\right\}, \tag{4}$$

where

$$\varepsilon_1 = \frac{\partial u}{\partial x}, \quad \varepsilon_2 = \frac{1}{r_0}\left(\frac{\partial v}{\partial\theta}-w\right), \quad \Omega = \frac{\partial v}{\partial x}+\frac{1}{r_0}\frac{\partial u}{\partial\theta}, \tag{5}$$

$$\kappa_1 = \frac{\partial^2 w}{\partial x^2}, \quad \kappa_2 = \frac{1}{r_0^2}\left(\frac{\partial^2 w}{\partial\theta^2}+\frac{\partial v}{\partial\theta}\right), \quad \tau = \frac{1}{r_0}\left(\frac{\partial^2 w}{\partial\theta\partial x}+\frac{\partial v}{\partial x}\right), \tag{6}$$

and $k_0^2 = h_0^2/12$. Note that, because we consider an inward normal for the 'elastic' part of the problem, the signs in the K_2 and τ equations for ε_2 K_2 and ϕ differ from those in Love's work.

Eq. (4), along with the expression for the kinetic energy per unit area of the shell E_k,

$$E_k = \frac{1}{2}\rho_s h_0\left\{\left(\frac{\partial u}{\partial t}\right)^2+\left(\frac{\partial v}{\partial t}\right)^2+\left(\frac{\partial w}{\partial t}\right)^2\right\}, \tag{7}$$

is used to derive the equations of shell dynamics using Hamilton's principle.

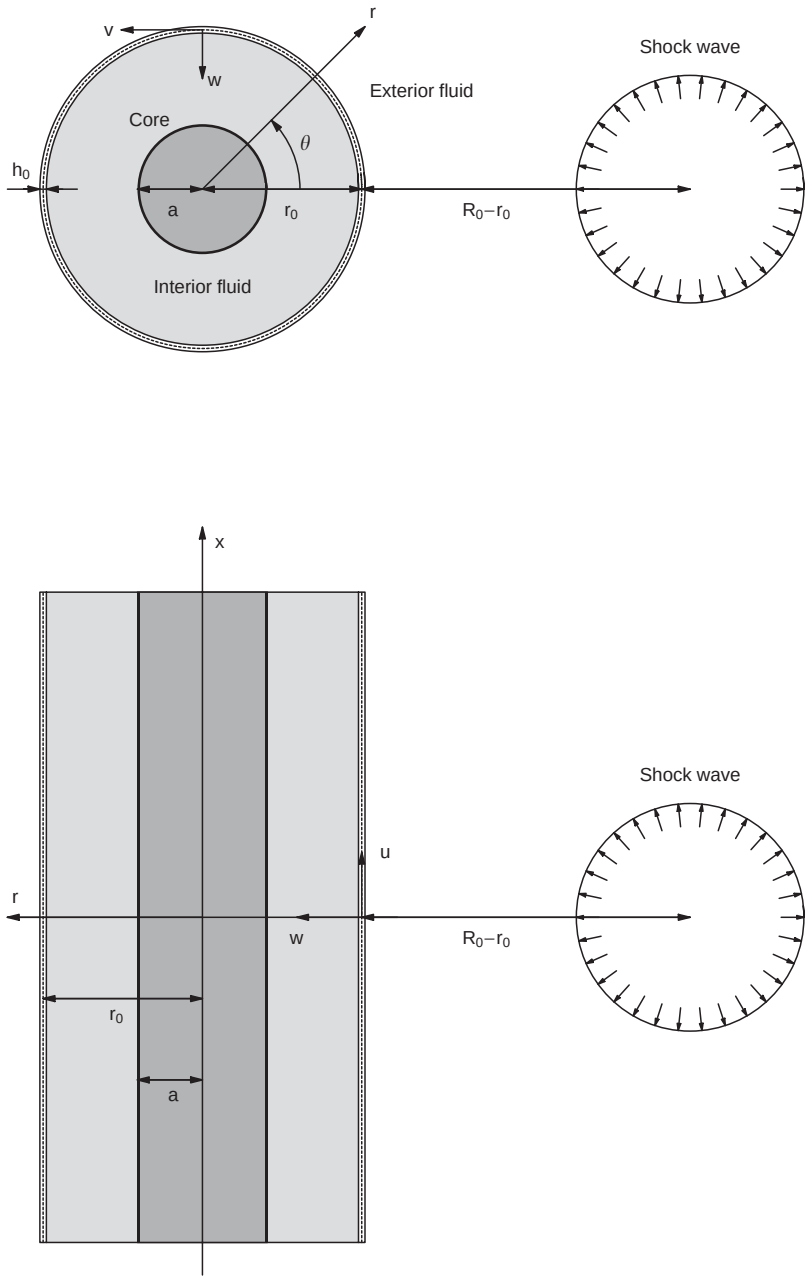

Fig. 1. Geometry of the problem.

The shell surface is subjected to a hydrodynamic load p consisting of the incident pressure p_0, diffraction pressure p_d, external radiation pressure p_r^e, and internal radiation pressure p_r^i,

$$p = p_0 + p_d + p_r^e + p_r^i. \tag{8}$$

The total fluid potential is

$$\phi = \phi_0 + \phi_d + \phi_r^e + \phi_r^i, \tag{9}$$

where ϕ_0, ϕ_d, ϕ_r^e, and ϕ_r^i are the potentials in the incident shock wave, diffracted wave, external radiated wave, and internal radiated wave, respectively. Then, the surface pressure components are

$$p_0 = -\rho_e \frac{\partial \phi_0}{\partial t}\bigg|_{r=r_0}, \qquad p_d = -\rho_e \frac{\partial \phi_d}{\partial t}\bigg|_{r=r_0}, \qquad p_r^e = -\rho_e \frac{\partial \phi_r^e}{\partial t}\bigg|_{r=r_0}, \tag{10}$$

and

$$p_r^i = -\rho_i \frac{\partial \phi_r^i}{\partial t}\bigg|_{r=r_0}. \tag{11}$$

The fluid velocity potential in a spherical step-exponential shock wave in the introduced cylindrical coordinates is

$$\phi_0 = -\frac{\lambda p_\alpha S_R}{\rho_e R}\{\mathrm{e}^{-(t-(R-R_0+r_0)c_e^{-1})\lambda^{-1}} - 1\}H(t-(R-R_0+r_0)c_e^{-1}), \tag{12}$$

where λ is the decay constant, p_α is the pressure in the front of the shock wave when it reaches the shell, $S_R = R_0 - r_0$ is the shock wave source stand off (the distance between the source and the surface of the shell), $R = \sqrt{R_0^2 + x^2 + r^2 - 2R_0 r\cos\theta}$ is the distance between the source of the shock wave and the point (x, r, θ) in the cylindrical coordinates, and $H(x)$ is the Heaviside unit step function

$$H(t) = \begin{cases} 1, & t \geqslant 0, \\ 0, & t < 0. \end{cases} \tag{13}$$

We assume that $t = 0$ at the moment when the wave front first reaches the shell. The parameters λ and p_α vary depending on R_0 and a few other factors [e.g., Cole (1948)].

The corresponding pressure on the shell surface is given by

$$p_0 = \frac{p_\alpha S_R}{R_1}\,\mathrm{e}^{-(t-(R_1-R_0+r_0)c_e^{-1})\lambda^{-1}} H(t-(R_1-R_0+r_0)c_e^{-1}), \tag{14}$$

where $R_1 = \sqrt{R_0^2 + x^2 + r_0^2 - 2R_0 r_0\cos\theta}$ is the distance between the source of the shock wave and the point (x, θ) on the shell surface.

Due to the very high-frequency nature of the interaction, it appears to be more convenient to deal with dimensionless variables, at least when it comes to a dynamic analysis. We normalize all the variables of the problem to r_0, c_e, and ρ_e, as outlined in the Nomenclature (a bar above a dimensionless variable distinguishes it from its dimensional counterpart). In particular, for such a choice of dimensionless variables it takes two dimensionless time units for a shock wave to move over the shell. From here on, dimensionless variables are used throughout the paper, with the analysis of the stress state being the only exception (stresses expressed in Pascals seem to be easier to relate to engineering practice than their dimensionless counterparts).

Before we move on to the formulation of the boundary and initial conditions, we re-state the problem in the introduced dimensionless form. The dimensionless wave equations are

$$\nabla^2 \bar{\phi}_e = \frac{\partial^2 \bar{\phi}_e}{\partial \bar{t}^2} \tag{15}$$

and

$$\nabla^2 \bar{\phi}_i = \frac{1}{\bar{c}_i^2}\frac{\partial^2 \bar{\phi}_i}{\partial \bar{t}^2}, \tag{16}$$

and the dimensionless hydrodynamic pressures are given by

$$\bar{p}_e = -\frac{\partial \bar{\phi}_e}{\partial \bar{t}} \quad \text{and} \quad \bar{p}_i = -\bar{\rho}_i \frac{\partial \bar{\phi}_i}{\partial \bar{t}}. \tag{17}$$

The dimensionless potential and kinetic energies are

$$\bar{E}_p = \frac{\bar{E}\bar{h}_0}{2(1-\nu^2)}\left\{\bar{\varepsilon}_1^2 + \bar{\varepsilon}_2^2 + 2\nu\bar{\varepsilon}_1\bar{\varepsilon}_2 + \frac{1}{2}(1-\nu)\bar{\Omega}^2 + \bar{k}_0^2(\bar{\kappa}_1^2 + \bar{\kappa}_2^2 + 2\nu\bar{\kappa}_1\bar{\kappa}_2 + 2(1-\nu)\bar{\tau}^2)\right\} \tag{18}$$

and

$$\bar{E}_k = \frac{1}{2}\,\bar{\rho}_s \bar{h}_0 \left\{ \left(\frac{\partial \bar{u}}{\partial \bar{t}}\right)^2 + \left(\frac{\partial \bar{v}}{\partial \bar{t}}\right)^2 + \left(\frac{\partial \bar{w}}{\partial \bar{t}}\right)^2 \right\}, \tag{19}$$

respectively, where

$$\bar{\varepsilon}_1 = \frac{\partial \bar{u}}{\partial \bar{x}}, \quad \bar{\varepsilon}_2 = \frac{\partial \bar{v}}{\partial \theta} - \bar{w}, \quad \bar{\Omega} = \frac{\partial \bar{v}}{\partial \bar{x}} + \frac{\partial \bar{u}}{\partial \theta}, \tag{20}$$

$$\bar{\kappa}_1 = \frac{\partial^2 \bar{w}}{\partial \bar{x}^2}, \quad \bar{\kappa}_2 = \frac{\partial^2 \bar{w}}{\partial \theta^2} + \frac{\partial \bar{v}}{\partial \theta}, \quad \bar{\tau} = \frac{\partial^2 \bar{w}}{\partial \theta \partial \bar{x}} + \frac{\partial \bar{v}}{\partial \bar{x}}. \tag{21}$$

The total dimensionless fluid velocity potential and hydrodynamic pressure on the shell surface are

$$\bar{p} = \bar{p}_0 + \bar{p}_d + \bar{p}_r^e + \bar{p}_r^i, \tag{22}$$

$$\bar{\phi} = \bar{\phi}_0 + \bar{\phi}_d + \bar{\phi}_r^{\,e} + \bar{\phi}_r^{\,i}, \tag{23}$$

where

$$\bar{p}_0 = -\frac{\partial \bar{\phi}_0}{\partial \bar{t}}\bigg|_{\bar{r}=1}, \qquad \bar{p}_d = -\frac{\partial \bar{\phi}_d}{\partial \bar{t}}\bigg|_{\bar{r}=1}, \qquad \bar{p}_r^e = -\frac{\partial \bar{\phi}_r^{\,e}}{\partial \bar{t}}\bigg|_{\bar{r}=1}, \tag{24}$$

and

$$\bar{p}_r^i = -\bar{\rho}_i \frac{\partial \bar{\phi}_r^{\,i}}{\partial \bar{t}}\bigg|_{\bar{r}=1}. \tag{25}$$

Finally, we state the boundary and initial conditions, and this completes the formulation of the problem. Shell dynamics is coupled to the dynamics of the fluids through the boundary conditions on the shell surface

$$\frac{\partial \bar{\phi}_r^{\,e}}{\partial \bar{r}}\bigg|_{\bar{r}=1} = -\frac{\partial \bar{w}}{\partial \bar{t}} \tag{26}$$

and

$$\frac{\partial \bar{\phi}_r^{\,i}}{\partial \bar{r}}\bigg|_{\bar{r}=1} = -\frac{\partial \bar{w}}{\partial \bar{t}}. \tag{27}$$

For the diffraction pressure we have

$$\frac{\partial \bar{\phi}_d}{\partial \bar{r}}\bigg|_{\bar{r}=1} = -\frac{\partial \bar{\phi}_0}{\partial \bar{r}}\bigg|_{\bar{r}=1}, \tag{28}$$

and also

$$(\bar{\phi}_d + \bar{\phi}_r^{\,e}) \longrightarrow 0 \quad \text{when } \bar{r} \to \infty. \tag{29}$$

The boundary condition on the surface of the core is

$$\frac{\partial \bar{\phi}_r^{\,i}}{\partial \bar{r}}\bigg|_{\bar{r}=\bar{a}} = 0. \tag{30}$$

To formulate the boundary conditions with respect to $\bar{x}$, we make use of the fact that the hydrodynamic waves in the fluids and elastic waves in the shell both have a finite velocity of propagation. Therefore, we can introduce a large enough parameter L and state the boundary conditions at $\bar{x} = \pm\bar{L}$ for the displacements as

$$\frac{\partial \bar{u}}{\partial \bar{x}}\bigg|_{\bar{x}=\pm\bar{L}} = 0, \quad \bar{v}|_{\bar{x}=\pm\bar{L}} = 0, \quad \bar{w}|_{\bar{x}=\pm\bar{L}} = 0, \frac{\partial^2 \bar{w}}{\partial \bar{x}^2}_{\bar{x}=\pm\bar{L}} = 0, \tag{31}$$

as well as zero boundary conditions for all potential components. We assume that the displacements and potentials are periodic with respect to θ, and we also assume zero initial conditions.

3. Hydrodynamics

We approach all the components of the hydrodynamic pressure with a uniform methodology. First, we apply the Laplace transform with respect to time to the wave equations written in the cylindrical coordinates to arrive at

$$\frac{\partial^2 \bar{\Phi}_e}{\partial \bar{r}^2} + \frac{1}{\bar{r}} \frac{\partial \bar{\Phi}_e}{\partial \bar{r}} + \frac{\partial^2 \bar{\Phi}_e}{\partial \bar{x}^2} + \frac{1}{\bar{r}^2} \frac{\partial^2 \bar{\Phi}_e}{\partial \theta^2} - s^2 \bar{\Phi}_e = 0 \tag{32}$$

and

$$\frac{\partial^2 \bar{\Phi}_i}{\partial \bar{r}^2} + \frac{1}{\bar{r}} \frac{\partial \bar{\Phi}_i}{\partial \bar{r}} + \frac{\partial^2 \bar{\Phi}_i}{\partial \bar{x}^2} + \frac{1}{\bar{r}^2} \frac{\partial^2 \bar{\Phi}_i}{\partial \theta^2} - \frac{s^2}{\bar{c}_i^2} \bar{\Phi}_i = 0. \tag{33}$$

Here $\bar{\Phi}_e$ and $\bar{\Phi}_i$ stand for the Laplace transforms of $\bar{\phi}_e$ and $\bar{\phi}_i$, respectively, and s is the transform variable.

Second, we apply separation of variables to the spatial coordinates. Making use of the boundary conditions for x and θ, and the radial boundary condition at infinity (29), we obtain the solutions of (32) and (33) as

$$\bar{\Phi}^e_{mn} = D_{mn} \mathrm{K}_n(\bar{r}\beta_m(s)) \cos(\tilde{m}\bar{x}) \cos(n\theta) \tag{34}$$

and

$$\bar{\Phi}^i_{mn} = \{F_{mn} \mathrm{I}_n(\bar{r}\beta_m(s\bar{c}_i^{-1})) + G_{mn} \mathrm{K}_n(\bar{r}\beta_m(s\bar{c}_i^{-1}))\} \cos(\tilde{m}\bar{x}) \cos(n\theta), \tag{35}$$

respectively. Here $m = 0, 1, ...,\ n = 0, 1, ...,\ \tilde{m} = (2m+1)\pi(2\bar{L})^{-1},\ \beta_m(s) = \sqrt{\tilde{m}^2 + s^2}$, I_n and K_n are the modified Bessel functions of order n of the first and second kind, respectively, and D_{mn}, F_{mn}, and G_{mn} are arbitrary functions of s.

Next, we determine the coefficients D_{mn}, F_{mn} and G_{mn} for each potential component. We expand the normal displacement $\bar{w}$ into a double series

$$\bar{w} = \sum_{m=0}^{\infty} \sum_{n=0}^{\infty} \bar{w}_{mn}(\bar{t}) \cos(\tilde{m}\bar{x}) \cos(n\theta), \tag{36}$$

as we do the incident pressure and the incident normal velocity on the shell surface,

$$\bar{p}_0 = \sum_{m=0}^{\infty} \sum_{n=0}^{\infty} \bar{p}^0_{mn}(\bar{t}) \cos(\tilde{m}\bar{x}) \cos(n\theta) \tag{37}$$

and

$$\left.\frac{\partial \bar{\phi}_0}{\partial \bar{r}}\right|_{\bar{r}=1} = \sum_{m=0}^{\infty} \sum_{n=0}^{\infty} \bar{b}_{mn}(\bar{t}) \cos(\tilde{m}\bar{x}) \cos(n\theta), \tag{38}$$

respectively, where

$$\bar{p}^0_{mn} = \frac{\Delta_{mn}}{\pi\bar{L}} \int_0^{\pi} \int_0^{\bar{L}} \bar{p}_0 \cos(\tilde{m}\bar{x}) \cos(n\theta)\, \mathrm{d}\bar{x}\, \mathrm{d}\theta, \tag{39}$$

$$\bar{b}_{mn} = \frac{\Delta_{mn}}{\pi\bar{L}} \int_0^{\pi} \int_0^{\bar{L}} \left.\frac{\partial \bar{\phi}_0}{\partial \bar{r}}\right|_{\bar{r}=1} \cos(\tilde{m}\bar{x}) \cos(n\theta)\, \mathrm{d}\bar{x}\, \mathrm{d}\theta, \tag{40}$$

and $\Delta_{m0} = 2$, $\Delta_{mn} = 4, n > 0$. Then, using the boundary conditions (26)–(28) and (30), we obtain the transforms of the harmonics of the potential components on the shell surface

$$\bar{\Phi}^d_{mn} = \bar{B}_{mn}(s) \Psi^e_{mn}(s) \cos(\tilde{m}\bar{x}) \cos(n\theta), \tag{41}$$

$$\bar{\Phi}^{r,e}_{mn} = s\bar{W}_{mn}(s) \Psi^e_{mn}(s) \cos(\tilde{m}\bar{x}) \cos(n\theta), \tag{42}$$

and

$$\bar{\Phi}^{r,i}_{mn} = -s\bar{W}_{mn}(s) \Psi^i_{mn}(s\bar{c}_i^{-1}) \cos(\tilde{m}\bar{x}) \cos(n\theta), \tag{43}$$

where $\bar{B}_{mn}$ and $\bar{W}_{mn}$ are the transforms of $\bar{b}_{mn}$ and $\bar{w}_{mn}$, respectively, and ψ^e_{mn} and ψ^i_{mn} are the 'response functions' of the problem with the Laplace transforms given by

$$\Psi^e_{mn}(s) = -\frac{\mathrm{K}_n(\beta_m(s))}{\beta_m(s)\mathrm{K}'_n(\beta_m(s))} \tag{44}$$

and

$$\Psi^i_{mn}(s) = \frac{1}{\beta_m(s)} \frac{\{\mathrm{I}'_n(a\beta_m(s))\mathrm{K}_n(\beta_m(s)) - \mathrm{K}'_n(a\beta_m(s))\mathrm{I}_n(\beta_m(s))\}}{\{\mathrm{K}'_n(\beta_m(s))\mathrm{I}'_n(a\beta_m(s)) - \mathrm{I}'_n(\beta_m(s))\mathrm{K}'_n(a\beta_m(s))\}}, \tag{45}$$

respectively. Recalling (3) and using some theorems related to the Laplace transform, the components of the pressure on the shell surface can now be obtained

$$\bar{p}_d = \sum_{m=0}^{\infty}\sum_{n=0}^{\infty} \bar{p}^d_{mn}(\bar{t})\cos(\tilde{m}\bar{x})\cos(n\theta), \tag{46}$$

$$\bar{p}^e_r = \sum_{m=0}^{\infty}\sum_{n=0}^{\infty} \bar{p}^{r,e}_{mn}(\bar{t})\cos(\tilde{m}\bar{x})\cos(n\theta), \tag{47}$$

and

$$\bar{p}^i_r = \sum_{m=0}^{\infty}\sum_{n=0}^{\infty} \bar{p}^{r,i}_{mn}(\bar{t})\cos(\tilde{m}\bar{x})\cos(n\theta), \tag{48}$$

where

$$\bar{p}^d_{mn}(\bar{t}) = -\bar{b}_{mn}(\bar{t}) - \int_0^{\bar{t}} \bar{b}_{mn}(\xi)\frac{\mathrm{d}\psi^e_{mn}}{\mathrm{d}\xi}(\bar{t}-\xi)\,\mathrm{d}\xi, \tag{49}$$

$$\bar{p}^{r,e}_{mn}(\bar{t}) = -\int_0^{\bar{t}} \frac{\mathrm{d}^2\bar{w}_{mn}(\xi)}{\mathrm{d}\xi^2}\,\psi^e_{mn}(\bar{t}-\xi)\,\mathrm{d}\xi, \tag{50}$$

and

$$\bar{p}^{r,i}_{mn}(\bar{t}) = \bar{\rho}_i\bar{c}_i\int_0^{\bar{t}} \frac{\mathrm{d}^2\bar{w}_{mn}(\xi)}{\mathrm{d}\xi^2}\,\psi^i_{mn}(\bar{c}_i(\bar{t}-\xi))\,\mathrm{d}\xi. \tag{51}$$

Hence, the total hydrodynamic pressure on the shell surface is

$$\bar{p} = \sum_{m=0}^{\infty}\sum_{n=0}^{\infty} \bar{p}_{mn}\cos(\tilde{m}\bar{x})\cos(n\theta), \tag{52}$$

where

$$\bar{p}_{mn} = \bar{p}^0_{mn} + \bar{p}^d_{mn} + \bar{p}^{r,e}_{mn} - \bar{p}^{r,i}_{mn}. \tag{53}$$

Note that because we consider an outward normal for both internal and external fluids, the internal radiation pressure is included in (53) with the opposite sign.

So far, the total pressure has been expressed in terms of the known pressure and fluid velocity in the shock wave, the response functions ψ^e_{mn} and ψ^i_{mn}, and the normal displacement of the shell surface $\bar{w}$. Now we will concentrate on the computation of the response functions.

It should be noted that the response functions only depend on the geometry of the problem, and not on the physical properties of the system. Therefore, once calculated, they can be used for any other problem with the same geometry, which makes the proposed approach quite attractive from the computational point of view. Indeed, when one is using Eqs. (49)–(53) to compute the hydrodynamic pressure for several systems with different parameters, a time-consuming numerical inversion of the Laplace transform is avoided. Thus, the methodology used here appears to have some advantages over the approaches where the displacements are obtained in the form of Laplace transforms, and the inversion is carried out at the very end.

To compute the response functions, we first express ψ^e_{mn} and ψ^i_{mn} in terms of the response functions of the related two-dimensional problem (i.e. the same system subjected to a plane shock wave), ψ^e_n and ψ^i_n, respectively,

$$\psi^e_{mn} = \psi^e_n(\bar{t}) - \tilde{m}\int_0^{\bar{t}} \psi^e_n\left(\sqrt{\bar{t}^2 - \xi^2}\right) \mathrm{J}_1(\tilde{m}\xi)\,\mathrm{d}\xi, \tag{54}$$

and

$$\psi^i_{mn} = \psi^i_n(\bar{t}) - \tilde{m}\int_0^{\bar{t}} \psi^i_n\left(\sqrt{\bar{t}^2 - \xi^2}\right) \mathrm{J}_1(\tilde{m}\xi)\,\mathrm{d}\xi, \tag{55}$$

where the Laplace transforms of ψ^e_n and ψ^i_n are given by

$$\Psi^e_n(s) = -\frac{\mathrm{K}_n(s)}{s\mathrm{K}'_n(s)}, \tag{56}$$

$$\Psi^i_n(s) = \frac{1}{s}\frac{\{\mathrm{I}'_n(as)\mathrm{K}_n(s) - \mathrm{K}'_n(as)\mathrm{I}_n(s)\}}{\{\mathrm{K}'_n(s)\mathrm{I}'_n(as) - \mathrm{I}'_n(s)\mathrm{K}'_n(as)\}}, \tag{57}$$

respectively, and J_1 is the Bessel function of the first order.

The functions ψ^e_n were introduced in the 1960s [e.g., Geers (1969)], and later appeared in many works examining the dynamics of cylindrical structures interacting with fluid. The inverse transform of (56) can be obtained both analytically and numerically. One of the possible approaches to the numerical inversion of (56) is discussed in Iakovlev (2001), including analysis of the errors associated with the inversion algorithm used. Fig. 2 shows ψ^e_n for various n.

A similar numerical procedure was used to compute ψ^i_n. Figs. 3 and 4 show ψ^i_1 for a few different values of $\bar{a}$, as well as ψ^i_1 for the same system without a core. The solid dots in these figures show the values of the functions at the points of finite discontinuity where all four functions have values equal to half of the sum of the right- and left-side limits at those points. See Iakovlev (2002b) for more information about this phenomenon, and also for a detailed investigation of the response functions for a fluid-filled shell without a core.

First of all, one can see that the functions ψ^i_n are much more complex and have significantly less regular behavior than the functions ψ^e_n. This is due to the fact that the physics of the interaction between the shell and the internal fluid is much more complex than that of the interaction with the external fluid, even if there is no core (multiple reflections of the internal hydrodynamic waves from the shell and/or core are responsible for this complexity). It should be particularly emphasized that, in the case of a shell with a core, the response functions only have points of finite

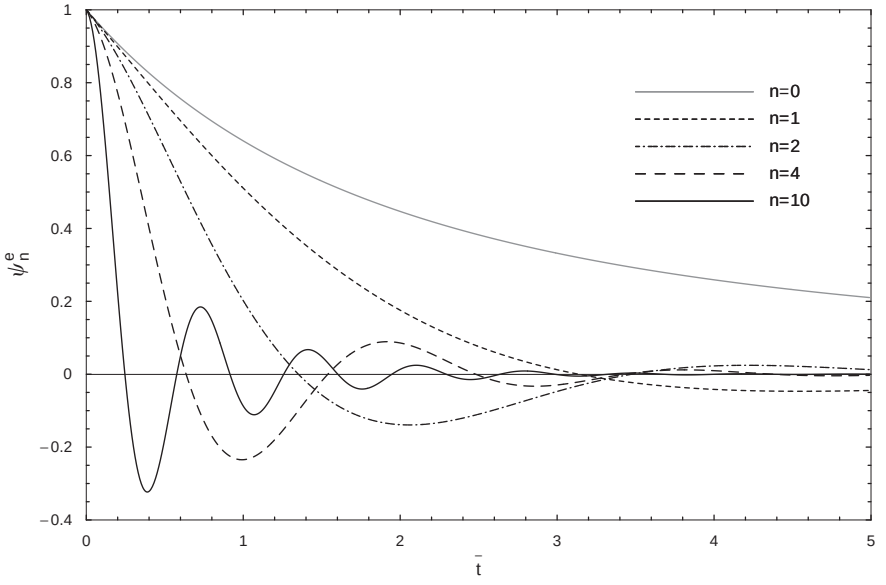

Fig. 2. The functions ψ^e_n for various n.

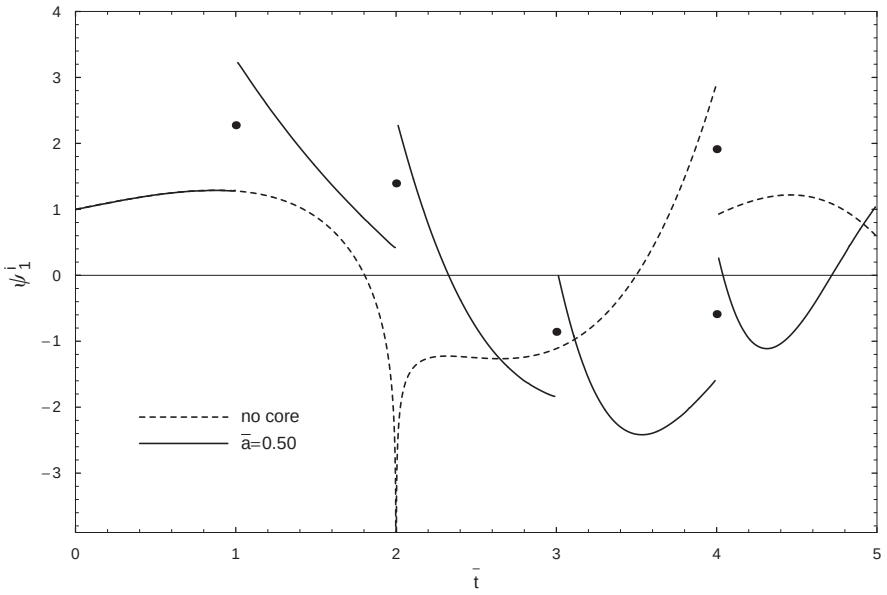

Fig. 3. The function ψ_1^i for the shell without a core and for the shell containing a core of radius $\bar{a} = 0.50$.

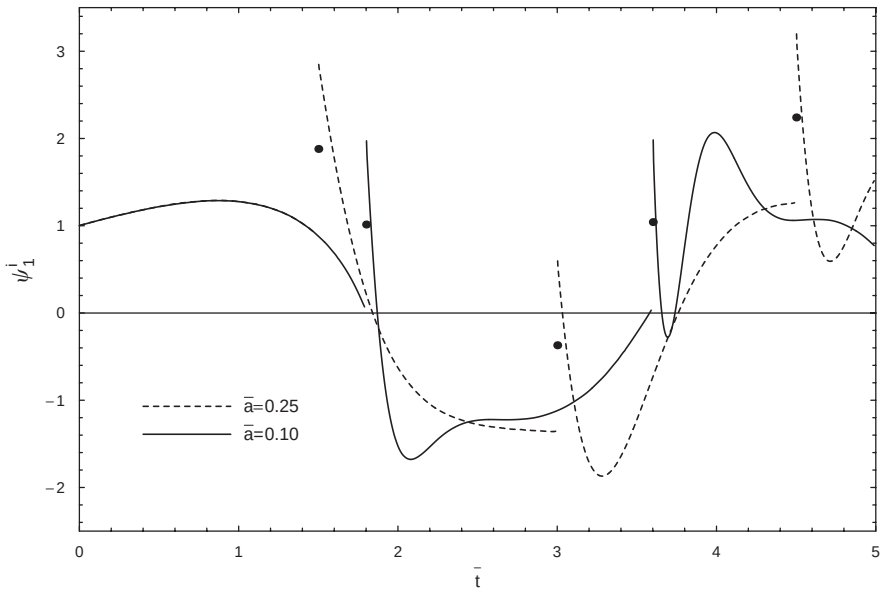

Fig. 4. The function ψ_1^i for shells containing cores of radii $\bar{a} = 0.25$ and 0.10.

discontinuity, and no singular points, whereas the response functions for the shell without a core have discontinuities of both types. This happens because the singular points represent the 'focusing' of the internal hydrodynamic wave at $\bar{r} = 0$ (on the axis of the shell), whereas when a core is placed coaxially within the shell, the focusing simply does not occur. Apparently, the finite discontinuities represent the reflections of hydrodynamic waves from the internal surfaces. Since there is one more internal surface when a core is present, the response functions for such a system have a larger number of points of finite discontinuity.

The timing of the occurrence of finite discontinuities is different for different cores, and the intervals between discontinuities are equal to the time necessary for a wave in the internal fluid to travel from the shell surface to the core

and back when the unit sound speed in the internal fluid is assumed, that is 1.90, 1.50, and 1.00 for the cores with the radii $\bar{a} = 0.10$, 0.25, and 0.50, respectively. In other words, the larger the radius of the core, the less time it takes for a wave to travel from the shell to the core, and therefore the more complex the wave pattern in the internal fluid is, and the more points of finite discontinuity the functions ψ_n^i have. Note that in the beginning of the process (i.e. when the shell does not 'know' about the core) all four functions are identical.

Generally speaking, the study of the response functions for the considered class of fluid–structure interaction problems appears to be of theoretical interest since the functions seem to capture the most important physical features of the interaction. They also seem to increase the efficiency of numerical computations, and make the corresponding algorithms significantly more versatile.

4. Structural dynamics

We are looking for the displacements in the form of double Fourier series as

$$\bar{u} = \sum_{m=0}^{\infty} \sum_{n=0}^{\infty} \bar{u}_{mn}(\bar{t}) \sin(\tilde{m}\bar{x}) \cos(n\theta), \tag{58}$$

$$\bar{v} = \sum_{m=0}^{\infty} \sum_{n=0}^{\infty} \bar{v}_{mn}(\bar{t}) \cos(\tilde{m}\bar{x}) \sin(n\theta), \tag{59}$$

and

$$\bar{w} = \sum_{m=0}^{\infty} \sum_{n=0}^{\infty} \bar{w}_{mn}(\bar{t}) \cos(\tilde{m}\bar{x}) \cos(n\theta). \tag{60}$$

The stresses in the shell are given by [e.g., Ugural (1981)]

$$\sigma_{11} = \sigma_{11}^0 + \sigma_{11}^b, \tag{61}$$

$$\sigma_{22} = \sigma_{22}^0 + \sigma_{22}^b, \tag{62}$$

and

$$\sigma_{12} = \sigma_{12}^0 + \sigma_{12}^b, \tag{63}$$

where σ_{11}, σ_{22}, and σ_{12} are the longitudinal (axial), transverse (azimuthal), and shear stresses, respectively. The membrane stress components σ_{11}^0, σ_{22}^0, and σ_{12}^0 are given by

$$\sigma_{11}^0 = \frac{E}{1-\nu^2}\left(\frac{\partial u}{\partial x} + \frac{\nu}{r_0}\frac{\partial v}{\partial \theta} - \frac{\nu}{r_0} w\right), \tag{64}$$

$$\sigma_{22}^0 = \frac{E}{1-\nu^2}\left(\frac{1}{r_0}\frac{\partial v}{\partial \theta} - \frac{w}{r_0} + \nu\frac{\partial u}{\partial x}\right), \tag{65}$$

and

$$\sigma_{12}^0 = \frac{E}{2(1+\nu)}\left(\frac{\partial v}{\partial x} + \frac{1}{r_0}\frac{\partial u}{\partial \theta}\right), \tag{66}$$

while the bending components σ_{11}^b, σ_{22}^b, and σ_{12}^b are

$$\sigma_{11}^b = \frac{zE}{1-\nu^2}\left(\frac{\partial^2 w}{\partial x^2} + \frac{\nu}{r_0^2}\frac{\partial v}{\partial \theta} + \frac{\nu}{r_0^2}\frac{\partial^2 w}{\partial \theta^2}\right), \tag{67}$$

$$\sigma_{22}^b = \frac{zE}{1-\nu^2}\left(\frac{1}{r_0^2}\frac{\partial v}{\partial \theta} + \frac{1}{r_0^2}\frac{\partial^2 w}{\partial \theta^2} + \nu\frac{\partial^2 w}{\partial x^2}\right), \tag{68}$$

and

$$\sigma_{12}^b = \frac{zE}{r_0(1+\nu)}\left(\frac{\partial v}{\partial x} + \frac{\partial^2 w}{\partial x \partial \theta}\right), \tag{69}$$

where z is the distance from the middle surface which varies from $-h_0/2$ on the inner surface to $h_0/2$ on the outer one. Note that Ugural (1981) considers z to be $-h_0/2$ on the outer surface and $h_0/2$ on the inner one, which is why in his work the bending terms are included in the equations for the compound stresses with a minus sign.

Stresses (61)–(63) can easily be expanded into double series similar to (58)–(60), and as long as the time-dependent displacement coefficients $\bar{u}_{mn}$, $\bar{v}_{mn}$, and $\bar{w}_{mn}$ are known, the three-dimensional stress–strain state of the shell can be simulated.

Before we proceed to the analysis of the stress–strain state, an important question has to be answered. Namely, how significant is the contribution of the bending terms? For any particular x and θ, the bending terms reach their maxima on either the inner or outer surface of the shell (the absolute maxima are considered here),

$$\sigma_{11}^{b,\max} = \frac{h_0 E}{2(1-\nu^2)}\left|\frac{\partial^2 w}{\partial x^2} + \frac{\nu}{r_0^2}\frac{\partial v}{\partial \theta} + \frac{\nu}{r_0^2}\frac{\partial^2 w}{\partial \theta^2}\right|, \tag{70}$$

$$\sigma_{22}^{b,\max} = \frac{h_0 E}{2(1-\nu^2)}\left|\frac{1}{r_0^2}\frac{\partial v}{\partial \theta} + \frac{1}{r_0^2}\frac{\partial^2 w}{\partial \theta^2} + \nu\frac{\partial^2 w}{\partial x^2}\right|, \tag{71}$$

$$\sigma_{12}^{b,\max} = \frac{h_0 E}{2r_0(1+\nu)}\left|\frac{\partial v}{\partial x} + \frac{\partial^2 w}{\partial x \partial \theta}\right|, \tag{72}$$

and so we have to compare (70)–(72) to the corresponding membrane stresses.

A preliminary analysis was carried out, and it appears that the maximum magnitudes of the bending components do not exceed 30% of those of the corresponding membrane components. It also seems that the bending terms exhibit somewhat 'irregular' behavior, that is high-magnitude bending stresses appear to be localized in certain regions, being considerably lower in the rest of the shell. Therefore, analyzing the bending terms in the context of the compound stresses, it appears that we are observing local second-order 'additions' to the membrane stresses provided by the bending terms rather than a 'steady' contribution that significantly changes the stress state. Thus, for the system considered here, it seems reasonable to say that the membrane stresses alone capture the most important dynamic features of the stress state quite well.

To thoroughly understand the dynamics of the bending stresses, much more detailed study is needed, which is beyond the scope of this paper. For our purposes, we will assume that

$$\sigma_{11} \approx \frac{E}{1-\nu^2}\left(\frac{\partial u}{\partial x} + \frac{\nu}{r_0}\frac{\partial v}{\partial \theta} - \frac{\nu}{r_0}w\right), \tag{73}$$

$$\sigma_{22} \approx \frac{E}{1-\nu^2}\left(\frac{1}{r_0}\frac{\partial v}{\partial \theta} - \frac{w}{r_0} + \nu\frac{\partial u}{\partial x}\right), \tag{74}$$

and

$$\sigma_{12} \approx \frac{E}{2(1+\nu)}\left(\frac{\partial v}{\partial x} + \frac{1}{r_0}\frac{\partial u}{\partial \theta}\right). \tag{75}$$

We should also mention that there are certain purely computational difficulties associated with evaluation of the bending terms. For example, Eqs. (67)–(69) involve second derivatives of the displacements, which translates into high-magnitude coefficients in the corresponding double series when m and/or n are large. As a result, the convergence of these series is much worse than that of the series describing the membrane stresses. This imposes considerably stricter requirements on the number of terms that have to be kept in the series to obtain a reasonably good approximation. Computationally this is quite a significant disadvantage, and another reason to limit the study to the membrane stresses only.

As we have mentioned before, stresses are the only variables in the paper that are analyzed in the dimensional form (even though as functions of *dimensionless* time and space coordinates).

Assuming the series representation of displacements (58)–(60), we derive the equations of shell dynamics. We first rewrite (20) and (21), omitting the sine and cosine factors, in terms of $\bar{u}_{mn}\sin(\tilde{m}\bar{x})\cos(n\theta)$, $\bar{v}_{mn}\cos(\tilde{m}\bar{x})\sin(n\theta)$, and $\bar{w}_{mn}\cos(\tilde{m}\bar{x})\cos(n\theta)$

$$\bar{\varepsilon}_1 = \bar{u}_{mn}\tilde{m}, \quad \bar{\varepsilon}_2 = \bar{v}_{mn}n - \bar{w}_{mn}, \quad \bar{\Omega} = -\bar{v}_{mn}\tilde{m} - \bar{u}_{mn}n, \tag{76}$$

$$\bar{\kappa}_1 = -\bar{w}_{mn}\tilde{m}, \quad \bar{\kappa}_2 = -\bar{w}_{mn}n^2 + \bar{v}_{mn}n, \ \bar{\tau} = \bar{w}_{mn}\tilde{m}n - \bar{v}_{mn}\tilde{m}. \tag{77}$$

Next, we express the strain and kinetic energy (18) and (19) in terms of the harmonics of the displacements ($\bar{u}_{mn}$, $\bar{v}_{mn}$, and $\bar{w}_{mn}$), integrate these expressions over the shell surface, and apply Hamilton's principle to obtain the following system of integro-differential equations for each combination of m and n, $m = 0, 1, ...$, and $n = 0, 1, ...$:

$$\begin{aligned}
&\gamma^2 \frac{\mathrm{d}^2\bar{u}_{mn}}{\mathrm{d}\bar{t}^2} + c_{mn}^{11}\bar{u}_{mn} + c_{mn}^{12}\bar{v}_{mn} + c_{mn}^{13}\bar{w}_{mn} = 0,\\
&\gamma^2 \frac{\mathrm{d}^2\bar{v}_{mn}}{\mathrm{d}\bar{t}^2} + c_{mn}^{21}\bar{u}_{mn} + c_{mn}^{22}\bar{v}_{mn} + c_{mn}^{23}\bar{w}_{mn} = 0,\\
&\gamma^2 \frac{\mathrm{d}^2\bar{w}_{mn}}{\mathrm{d}\bar{t}^2} + c_{mn}^{31}\bar{u}_{mn} + c_{mn}^{32}\bar{v}_{mn} + c_{mn}^{33}\bar{w}_{mn} = \chi\bar{p}_{mn},
\end{aligned} \tag{78}$$

where

$$\begin{aligned}
&c_{mn}^{11} = \frac{1-\nu}{2}n^2 + \tilde{m}^2, \quad c_{mn}^{12} = c_{mn}^{21} = \frac{1+\nu}{2}\tilde{m}n,\\
&c_{mn}^{13} = c_{mn}^{31} = -\nu\tilde{m},\\
&c_{mn}^{22} = \frac{1-\nu}{2}\tilde{m}^2 + n^2 + \bar{k}_0^2(n^2 + (1-\nu)\tilde{m}^2),\\
&c_{mn}^{23} = c_{mn}^{32} = -n - \bar{k}_0^2(n^3 + n\tilde{m}^2),\\
&c_{mn}^{33} = 1 + \bar{k}_0^2(\tilde{m}^2 + n^2)^2,
\end{aligned} \tag{79}$$

$\gamma = \bar{c}_s^{-1}$, $\chi = (\bar{\rho}_s\bar{c}_s^2\bar{h}_0)^{-1}$, all initial conditions are zero, and the pressure $\bar{p}_{mn}$ is given by (53).

Systems (78) were approached numerically (finite differences), and the functions $\bar{u}_{mn}$, $\bar{v}_{mn}$ and $\bar{w}_{mn}$ were computed for $m = 0, ..., 200$ and $n = 0, ..., 40$.

5. Results and discussion

We consider a steel shell (the density of and the sound speed in the shell material are 7800 kg/m^3 and 5000 m/s, respectively), with thickness-to-radius ratio $h_0/r_0 = 0.01$ ($r_0 = 1$ m and $h_0 = 0.01$ m), submerged into water (the density and sound speed are 1000 kg/m^3 and 1400 m/s, respectively) and filled with oil (900 kg/m^3 and 1350 m/s). The stress–strain state of the shell is analyzed for three different cores with the radii $a = 0.10$ m ($\bar{a} = 0.10$), $a = 0.25$ m ($\bar{a} = 0.25$), and $a = 0.50$ m ($\bar{a} = 0.50$), which we refer to as the small-, medium-, and large-radius cores, respectively. The stress–strain state of the core-containing shell is then compared to that of the same shell without a core. We analyze the influence of a spherical shock wave with a 'distant' source, i.e. we assume that the distance between the source and the axis of the shell is equal to five radii of the shell ($\bar{R}_0 = 5.0$). The parameters λ and p_α for such a shock wave were estimated to be 0.0001314 s and 7.9 MPa, respectively [e.g., Cole (1948)].

For brevity, from here on we will refer to the point $\bar{x} = 0$, $\theta = 0$ (the point that first comes into contact with a shock wave) as the head point of the shell, and to the point $\bar{x} = 0$, $\theta = \pi$ (the point that is last reached by a shock wave) as the tail point.

We first focus on the normal displacement $\bar{w}$. Fig. 5 shows $\bar{w}$ at the head point. It seems that it makes more sense to analyze $\bar{w}/\bar{h}_0$ rather than $\bar{w}$. In particular, in this case it is very easy to see if the displacements obtained are in agreement with the assumptions of the linear theory of shells used (we will see that indeed they are for the considered shock wave). Since both w and h_0 are normalized to r_0, it does not matter which form of w/h_0, dimensional or dimensionless, we are considering. One can see that in the beginning of the interaction the displacements are identical for all four systems. The core starts to affect $\bar{w}$ when the hydrodynamic wave in the internal fluid originated at $\bar{t} \approx 0$ at the head point reflects from the core and comes back to the head point. This occurs at $\bar{t} \approx 1.0$, 1.5, and 1.9 for $\bar{a} = 0.50$, 0.25, and 0.10, respectively. The maximum displacement differs insignificantly between the shell without a core and the shells with the small- and medium-radius cores, and is about 15% lower for the shell with the large-radius core. In spite of the fact that the displacements have the same order of magnitude, the sudden change of $\bar{w}$ caused by the presence of a core leads to quite different dynamic features of the process. This difference is particularly noticeable for the time derivatives of $\bar{w}$.

Note that we can easily see if the numerically observed times of arrival of the first ('primary') core-reflected wave to the head point agree with the times one can predict theoretically knowing the sound speed in the shell material. Namely, if we adopt the notation t_c^1 for the time it takes for the hydrodynamic wave in the internal fluid to reach the core and for

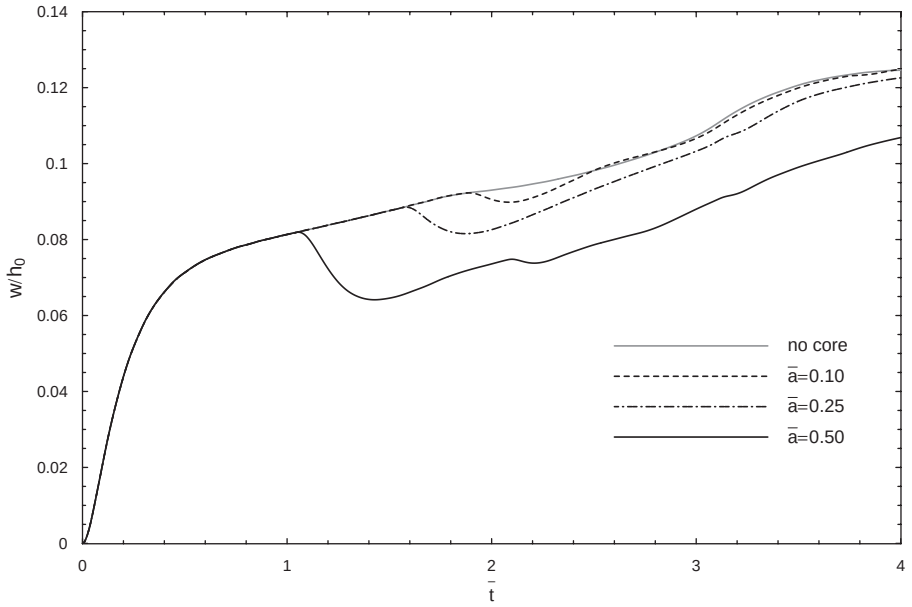

Fig. 5. Normal displacement at the head point.

the reflected wave to come back to the head point, we will have

$$\bar{t}_c^1 = \frac{2(1-\bar{a})}{\bar{c}_i}, \tag{80}$$

which gives us 1.04, 1.56, and 1.87 for $\bar{a} = 0.50$, $\bar{a} = 0.25$, and $\bar{a} = 0.10$, respectively. As one can see, these 'theoretically predicted' times agree very well with the numerically observed ones. As far as one is concerned about the validity of the solution proposed here, this is a very comforting result.

We can also predict the arrival time t_c^2 of the second core-reflected wave,

$$\bar{t}_c^2 = \frac{4(1-\bar{a})}{\bar{c}_i}, \tag{81}$$

which yields 2.07, 3.10, and 3.73 for $\bar{a} = 0.50$, $\bar{a} = 0.25$, and $\bar{a} = 0.10$, respectively. The influence of this wave on $\bar{w}$ is most pronounced for the large-radius core, and one can notice a low-magnitude peak of $\bar{w}$ at the time which is very close to the one predicted by Eq. (81). In the cases of the small- and medium-radius cores the influence of the secondary wave is harder to see, at least from the plots presented here.

Fig. 6 shows the normal displacements at the tail point. The dynamics of $\bar{w}$ is very similar for the shell without a core and for the shell with the small- and medium-radius cores, whereas for the large-radius core $\bar{w}$ has a distinct peak at $\bar{t} \approx 2.3$. After $\bar{t} \approx 2.5$, the dynamics of $\bar{w}$ is very similar for all four systems, although the magnitudes are different.

To allow a better understanding of the dynamics of the interaction as well as the influence of a core, Figs. 7 and 8 show series of three-dimensional 'snapshots' of the shell with and without a core (only $\bar{w}$ is shown). One can see how the first core-reflected wave reaches the head point and originates the 'secondary' wave of $\bar{w}$ (which is not present in the no-core case). Note that the displacements shown were significantly enhanced to make the plots more illustrative. As one can see from Figs. 5 and 6, the magnitude of the actual $\bar{w}$ is always less than the thickness of the shell. Note also that $\bar{w}$ at the head and tail points has different signs, i.e. the surface of the shell bends inside at the head point and outside at the tail one.

Now we turn to the analysis of the stress state. Our primary focus will be on the transverse stress, since it appears to be the major contributor to the stress state. Although there are zones where the axial and/or shear stress locally prevail, the absolute maximum of the transverse stress is always significantly higher. More specifically, the absolute maxima of the axial and shear stresses usually do not exceed 50% and 30% of the absolute maximum of the transverse stress, respectively.

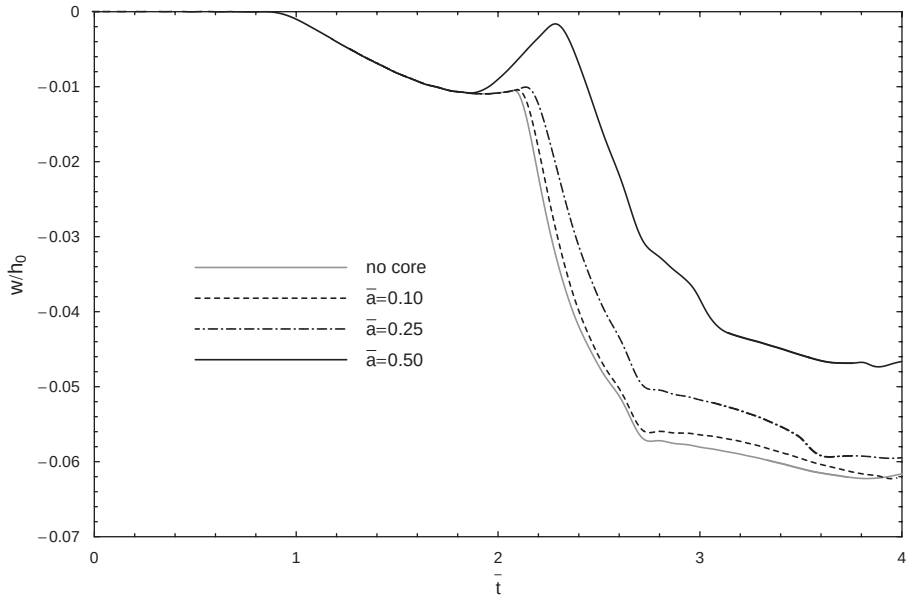

Fig. 6. Normal displacement at the tail point.

We start from the analysis of the transverse stress at the tail point (Fig. 9). Note that here we plot dimensional stresses versus dimensionless time/spatial coordinates. The stress has two distinct peaks of approximately the same magnitude, the first one (negative) at $\bar{t} \approx 1$ caused by the elastic waves propagating in the shell, and the second one (positive) at $\bar{t} \approx 2.2$ caused by the hydrodynamic wave propagating in the internal fluid. The stresses in the shell without a core and in the shells with the small- and medium-radius cores are very similar throughout the interaction. The stress in the shell with the large-radius core starts to differ at $\bar{t} \approx 1.8$, i.e. when the elastic wave originated in the proximity of the head point by the core-reflected hydrodynamic wave at $\bar{t} \approx 1$ arrives at the tail point. At $\bar{t} \approx 2$ the hydrodynamic wave in the internal fluid originated at the head point in the beginning of the interaction arrives at the tail point as well. However, unlike in the cases of the small- and medium-radius cores, the large-radius core occupies a significant part of the internal fluid volume, and it substantially changes the internal hydrodynamic pattern. In particular, the core noticeably 'dissipates' the hydrodynamic wave, and the wave does not have the same effect on the stress state as it did for the shells with the small- and medium-radius cores, and for the shell without a core. As a result, there is a considerable (about 35%) reduction of the second peak of the stress. Note that the second peak is tensile, whereas the first one is compressive. For $\bar{t} \geqslant 2.5$ the stresses are approximately the same for all four systems, although for the large-radius core the stress has two secondary small-magnitude peaks, apparently caused by multiple reflections of the internal hydrodynamic waves from the core.

Fig. 10 shows the transverse stress σ_{22} at the head point. As was the case with the displacements, during the initial period of the interaction the stresses are the same for all four systems. They start to differ when the core-reflected hydrodynamic wave reaches the head point. This wave does not have any significant influence on the stress for the small-radius core, causes noticeable but short-time peak in the case of the medium-radius core, and leads to a high-magnitude and relatively long-lasting peak in the case of the large-radius core ($\bar{t} \approx 1.4$). The stresses have a second peak at $\bar{t} \approx 1.9$ caused by the superposition of elastic waves that travel around the shell once and return to the head point. After a short transitional period when the dynamic patterns of the stress are similar for all four systems, the stress in the shell without a core experiences the third major peak (a positive one, $\bar{t} \approx 3.1$). This time it is caused by the superposition of the elastic waves originating at the tail point at $\bar{t} \approx 2.2$. The stresses in the shell without a core and in the shell with the small-radius core are almost identical. The peak for the shell with the medium-radius core is slightly shifted towards the larger times and its magnitude is about 20% lower (the core is large enough to affect, although not significantly, the distribution of the stress). For the large-radius core the third peak is completely eliminated. Note that although the third peak is smaller in magnitude than the two previous ones, it is the only considerable tensile stress at the head point. Thus, the large-radius core significantly reduces tensile stress at the head point. This result appears to be of interest for materials reacting differently to tension and compression. Note also that although the third peak is completely eliminated, another tensile peak, which is not present in other cases, is originated at $\bar{t} \approx 1.4$. For $\bar{t} \geqslant 3.5$ the stresses in

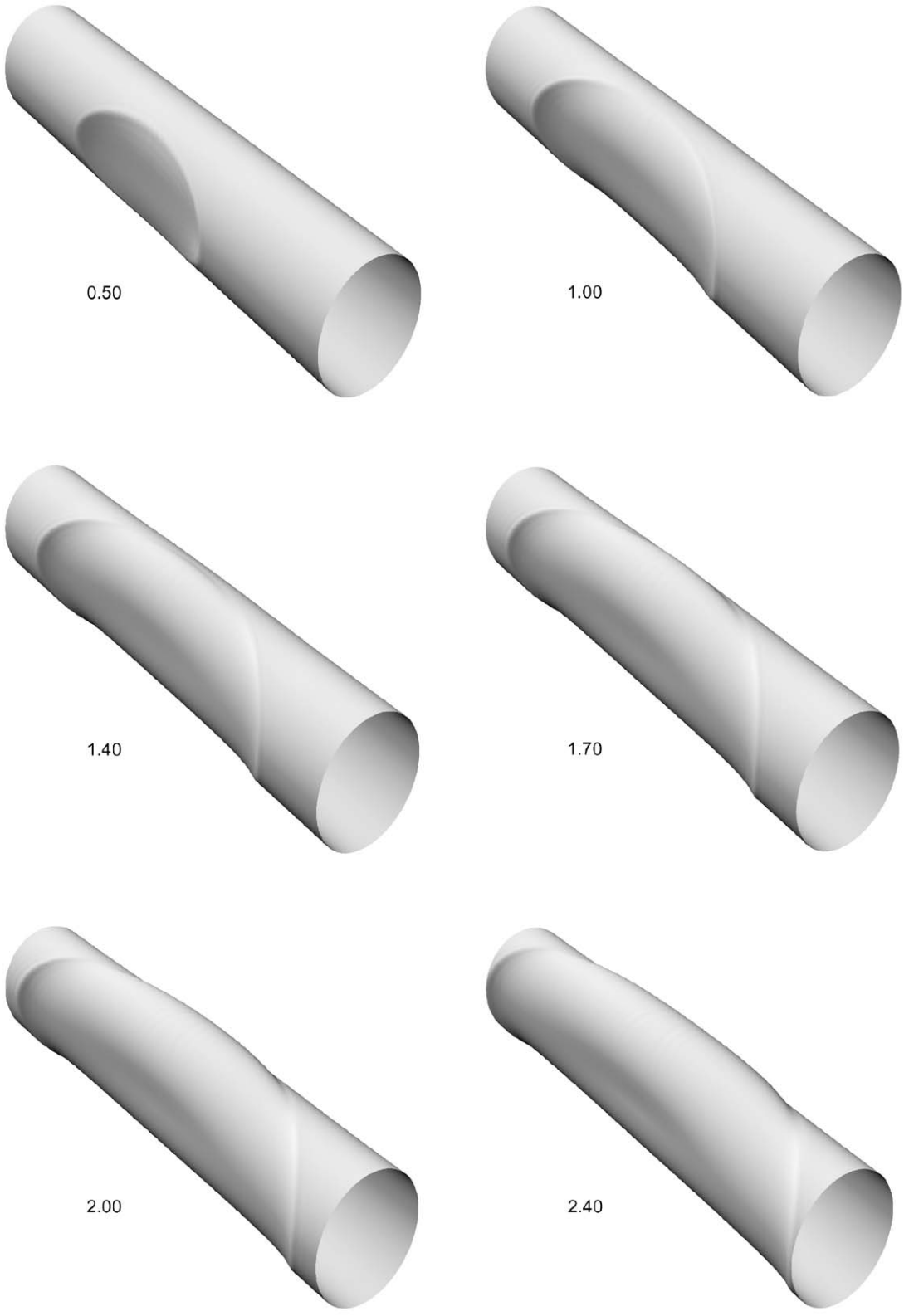

Fig. 7. Dynamics of the normal displacement for the shell without a core.

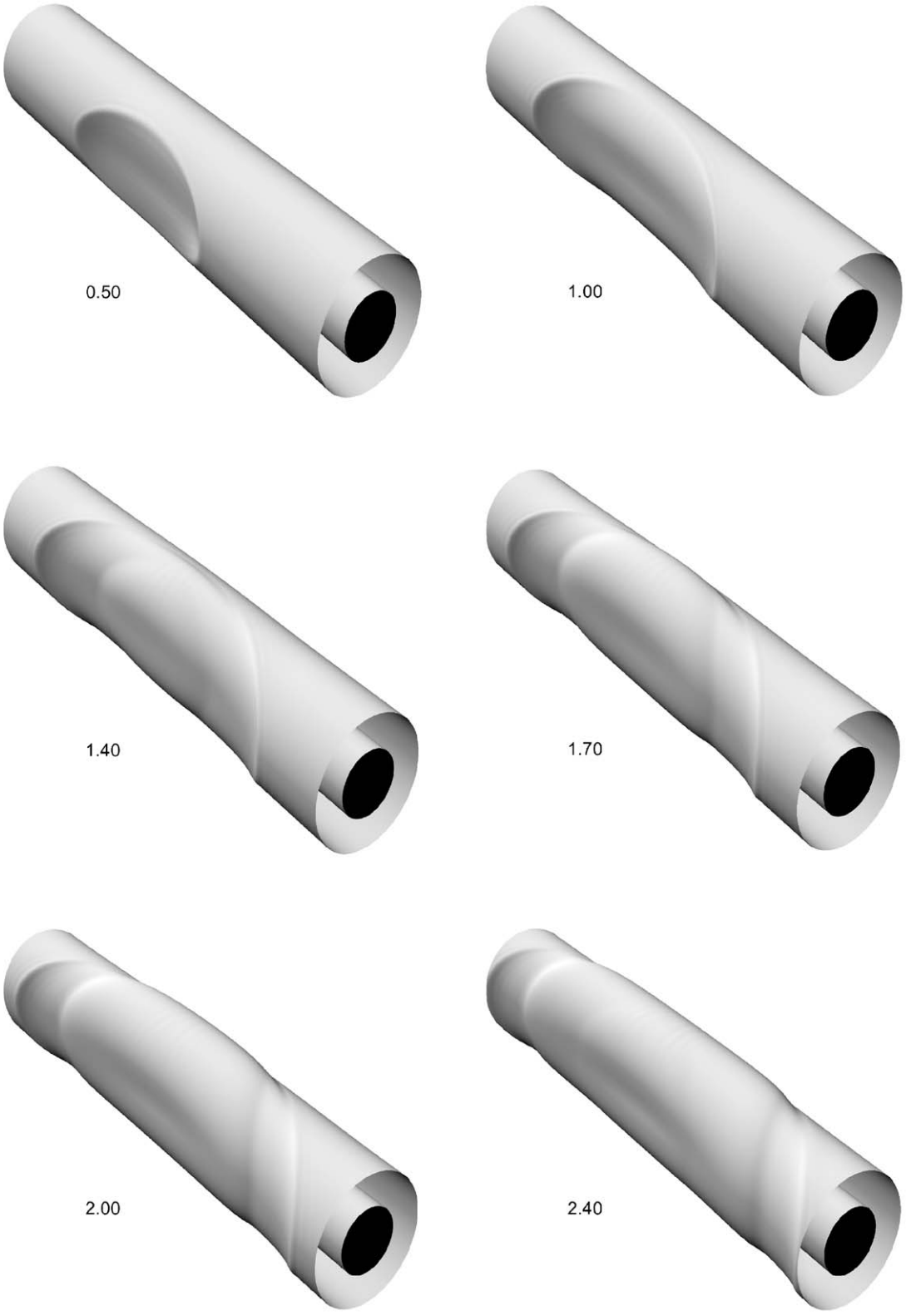

Fig. 8. Dynamics of the normal displacement for the shell with the large-radius core.

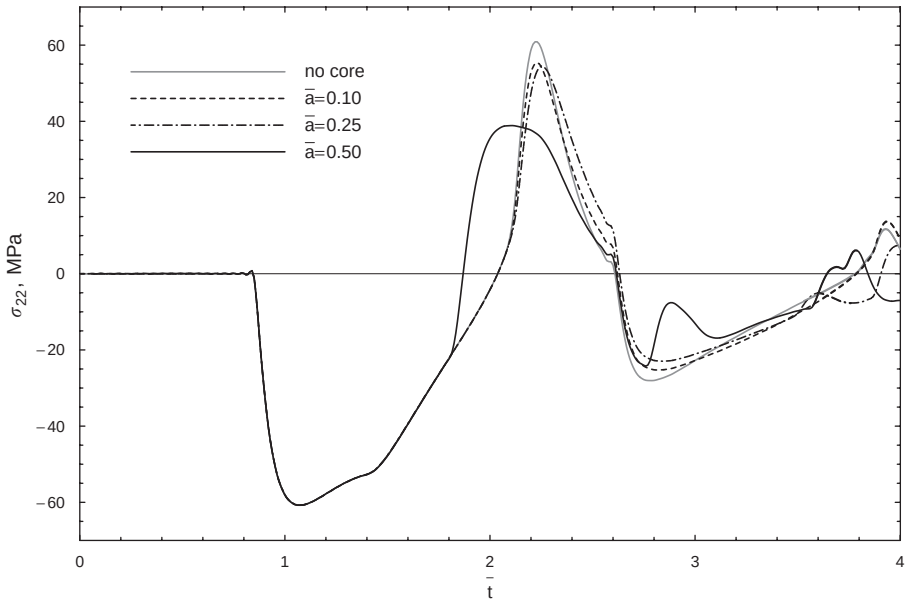

Fig. 9. Transverse stress at the tail point.

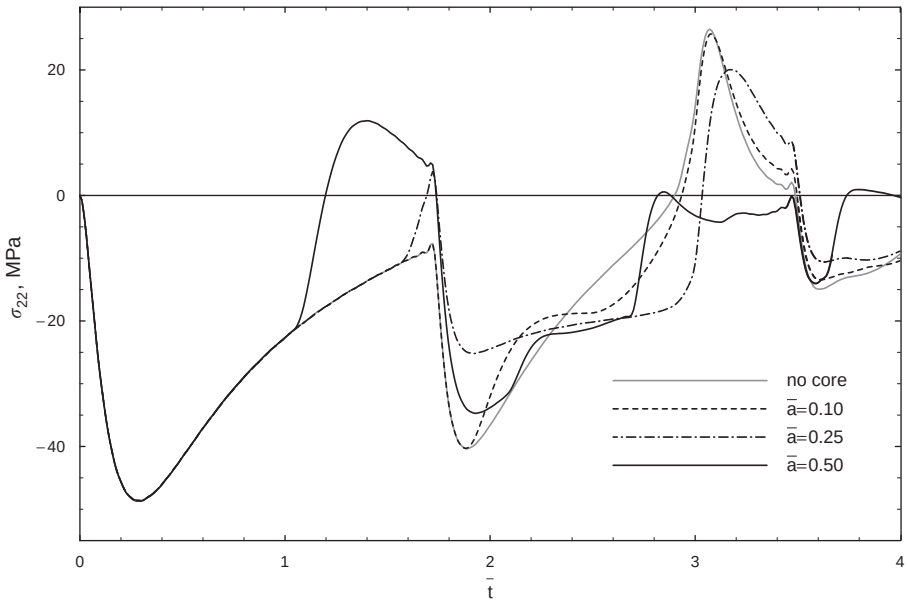

Fig. 10. Transverse stress at the head point.

the shell without a core and in the shells with the small- and medium-radius cores are very similar, whereas the stress in the shell with the large-radius core has a considerably lower magnitude.

It is also of interest to look at the distribution of the maximum stress magnitude over the entire shell surface. Fig. 11 shows the maximum magnitude of the transverse stress in each cross-section of the shell. As one can see, the most stressed cross-section is the middle one ($\bar{x} = 0$), and this is true for all four systems. The maximum stresses are identical in the proximity of $\bar{x} = 0$ ($-3 \leqslant \bar{x} \leqslant 3$), but at larger $\bar{x}$ they start to differ. Although these differences can be locally significant, their global effect it is not very important (local maxima at $|\bar{x}| > 3$ are always much lower than the maximum

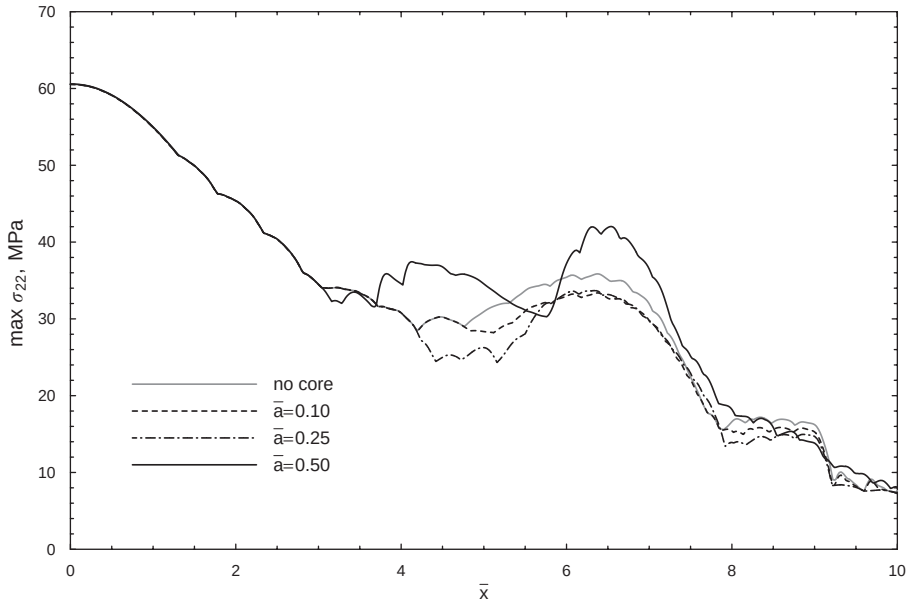

Fig. 11. Spatial distribution of the maximum magnitude of the transverse stress.

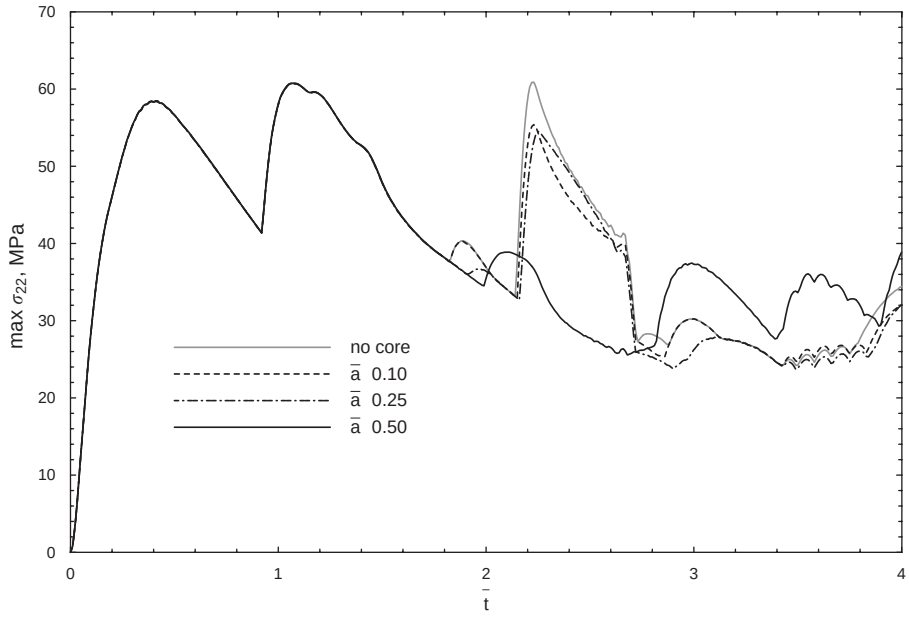

Fig. 12. Maximum magnitude of the transverse stress computed over the entire shell surface.

at $\bar{x} = 0$). Thus, we can state that when the global maximum of the transverse stress is the primary concern, the analysis should be focused on the middle cross-section. However, if the detailed study of the stress dynamics is being carried out, the stress state of the entire shell should be examined.

If the analysis of the spatial distribution of the maximum stress provides one with the information about the most stressed zones of the structure, the study of the distribution of the maximum stress in time allows for a better understanding of the complex dynamics of the stress state. Fig. 12 shows the absolute maximum of the magnitude of the transverse stress computed over the entire shell surface versus time. This plot is very informative, first

of all because it clearly illustrates the major dynamic features of the interaction. In particular, for the shell without a core, one can see three distinct peaks of the stress, each caused by a different physical phenomenon. The first peak at $\bar{t} \approx 0.5$ is caused by the direct action of the shock wave, the second at $\bar{t} \approx 1.1$ is caused by the superposition (at the tail point) of the elastic waves propagating in the shell, and the third one at $\bar{t} \approx 2.2$ is caused by the hydrodynamic wave propagating in the internal fluid. All three peaks have approximately the same magnitude (the difference does not exceed 5%). Note that, once again, this allows us to state that the maximum stress in fluid-interacting thin-walled cylindrical structures can be caused by *any* of the three mentioned phenomena, and the maximum can occur at virtually any time between dimensionless 0 and 2.5, depending on the parameters of the system. A very similar situation is observed for the shells with the small- and medium-radius cores. However, for these systems, the third peak is about 10% lower than the first two. In the case of the large-radius core the first two peaks are the same, whereas, because of the reasons outlined above, the third peak is no longer present.

Thus, the influence that a core has on the stress state of the shell is quite clear now, and we can conclude that a core only affects the third ('hydrodynamics-driven') peak. This happens because the first two peaks occur *before* the influence of a core becomes significant enough to cause any noticeable changes in the stress state. Note that Fig. 12 only shows the *magnitude* of the stress whereas in reality the first two peaks are negative (compressive stress), and the third one is positive (tensile stress).

Figs. 13 and 14 show the three-dimensional dynamics of the transverse stress in the shells without and with a core, respectively. Fig. 15 shows the details of the dynamics of the shell containing the large-radius core when the first core-reflected wave arrives at the head point. These two-dimensional 'snapshots' of an 'unwrapped' shell allow one to examine dynamic features that were not captured by other plots. In particular, one can see how the stress states start to differ when the first core-reflected wave arrives at the head point. Also, in the case of the large-radius core, one can see how this wave causes a significant area of tensile stress in the proximity of the head point at $\bar{t} \approx 1.3$–1.6. At the larger times the distribution of the stress is quite complex in all cases considered, and it becomes particularly irregular when a core is present.

Finally, Figs. 16 and 17 show the dynamic *distribution* of the magnitude of the transverse stress over the three-dimensional surface of the shell (the core is not shown). These figures are intended to complement the plots showing the 'unwrapped' shell (Figs. (13)–(15)) rather than replace them. The reds represent the highest magnitudes, and the blues show the magnitudes close to zero. Since the focus was on dynamic features rather than on quantitative analysis, the colors were assigned to stress magnitudes separately for each 'snapshot'.

A few previously discussed dynamic features are particularly obvious now. For example, it is easy to analyze the effect that the first core-reflected wave has on the stress state of the shell. After the wave arrives at the head point at $\bar{t} \approx 1$, it originates a 'second-order' wave of stress with a very pronounced circular front ($\bar{t} \approx 1.20$–1.35, the 'circular' nature of the wave front is particularly apparent at $\bar{t} \approx 1.30$–1.35). This wave interferes with the high-magnitude stress wave originated at the tail point and propagating in the direction of the head point ($\bar{t} \approx 1.40$–1.55). As a result, the 'circular' wave splits into two waves, one continuing to travel towards the tail point, and the other reversing back to the head point ($\bar{t} \approx 1.55$–1.65). The latter wave collapses as it reaches the head point at $\bar{t} \approx 1.75$. At approximately the same time, the high-magnitude stress waves coming from the tail point reach the head point as well. The waves constructively superpose which leads to a relatively high-magnitude stress at $\bar{t} \approx 1.85$–2.05. Finally, one can notice the arrival at the head point of the second core-reflected wave at $\bar{t} \approx 2.10$–2.25. Even though the amplitude of the corresponding stress wave is not nearly as high as that of the stress wave originated by the first core-reflected wave, this dynamic feature deserves some attention.

6. Conclusions

We have considered a thin submerged fluid-filled circular cylindrical shell containing a coaxial rigid cylindrical core and subjected to a spherical shock wave. There was a possibility that a core, even a small-radius one, will 'de-focus' the waves in the internal fluid and therefore will lead to a significant reduction of the maximum stress. The study carried out shows that this does not happen for small- and medium-radius cores ($a/r_0 \leqslant 0.25$). The stress reduction does not exceed 10% in such cases. However, a large-radius core ($a/r_0 \geqslant 0.40$) does lead to a significant (35% for $a/r_0 = 0.50$) reduction of the stress caused by the hydrodynamic effects in the internal fluid. It appears that a large-radius core 'dissipates' the hydrodynamic waves in the internal fluid, whereas small- and medium-radius cores seem to just slightly 're-distribute' the influence of the internal hydrodynamic shock load. In a way, it seems that the internal fluid works as a wave-guide which is very stable to local disturbances. The fluid layer between the shell and the core 'conducts' the hydrodynamic load with minimal losses even when the radius of the core is 25% of that of the shell. This result is somewhat the

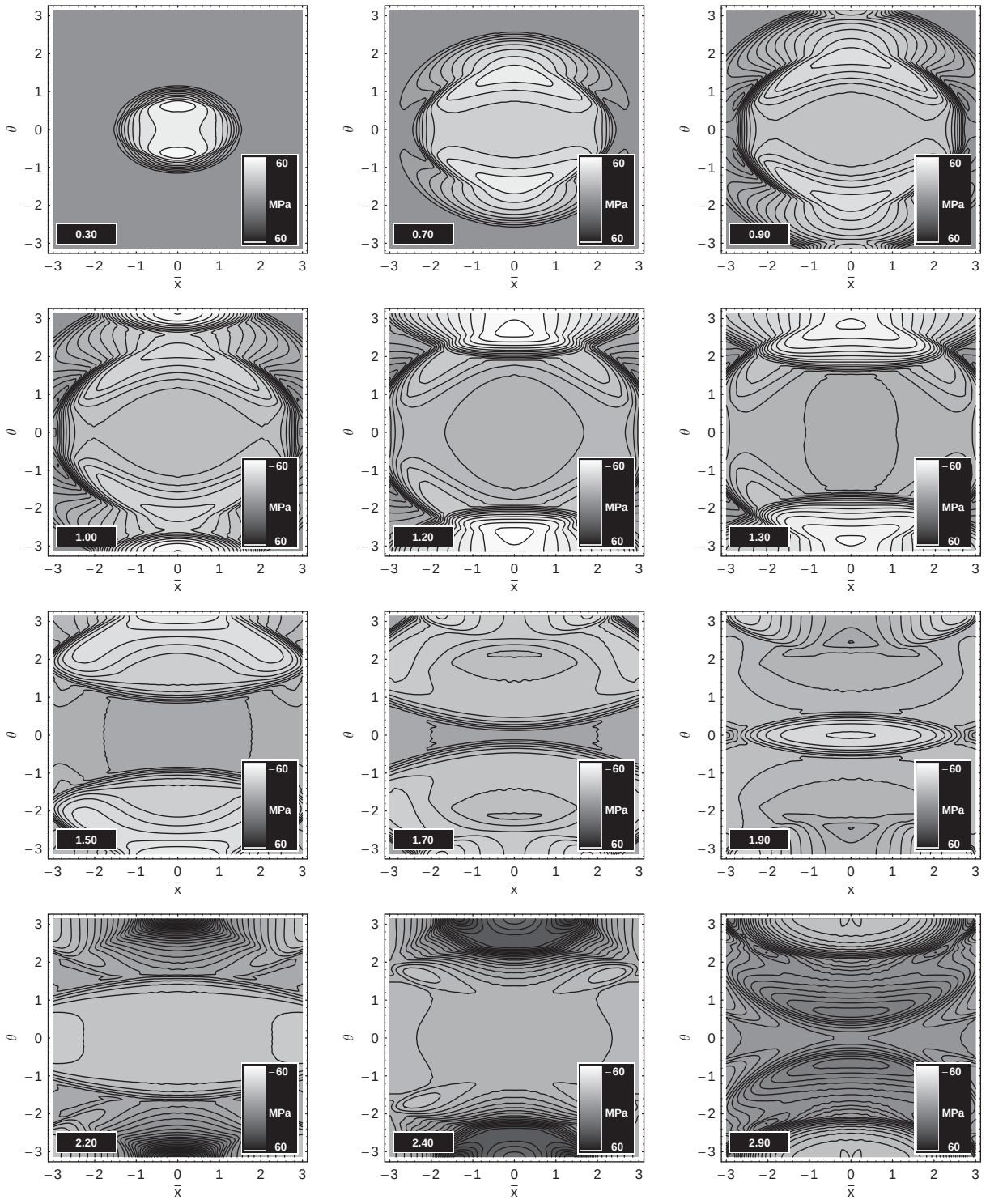

Fig. 13. Dynamics of the transverse stress in the shell without a core.

opposite of what was expected ('small-disturbance/large-stress-reduction'). This interesting feature of the system 'shell-fluid-core' should certainly be taken into consideration when one is designing constructively advanced systems involving shells and fluids.

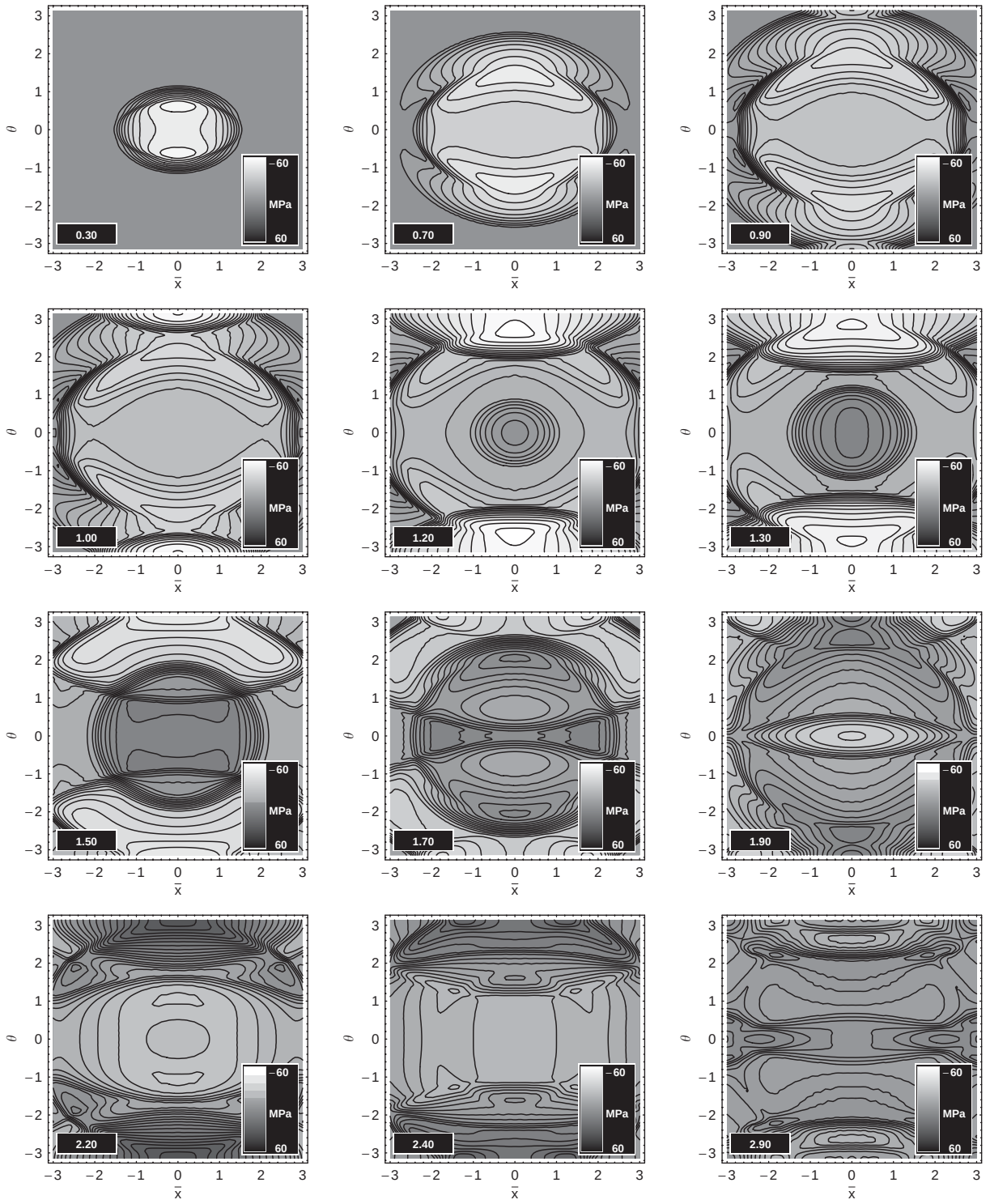

Fig. 14. Dynamics of the transverse stress in the shell with the large-radius core.

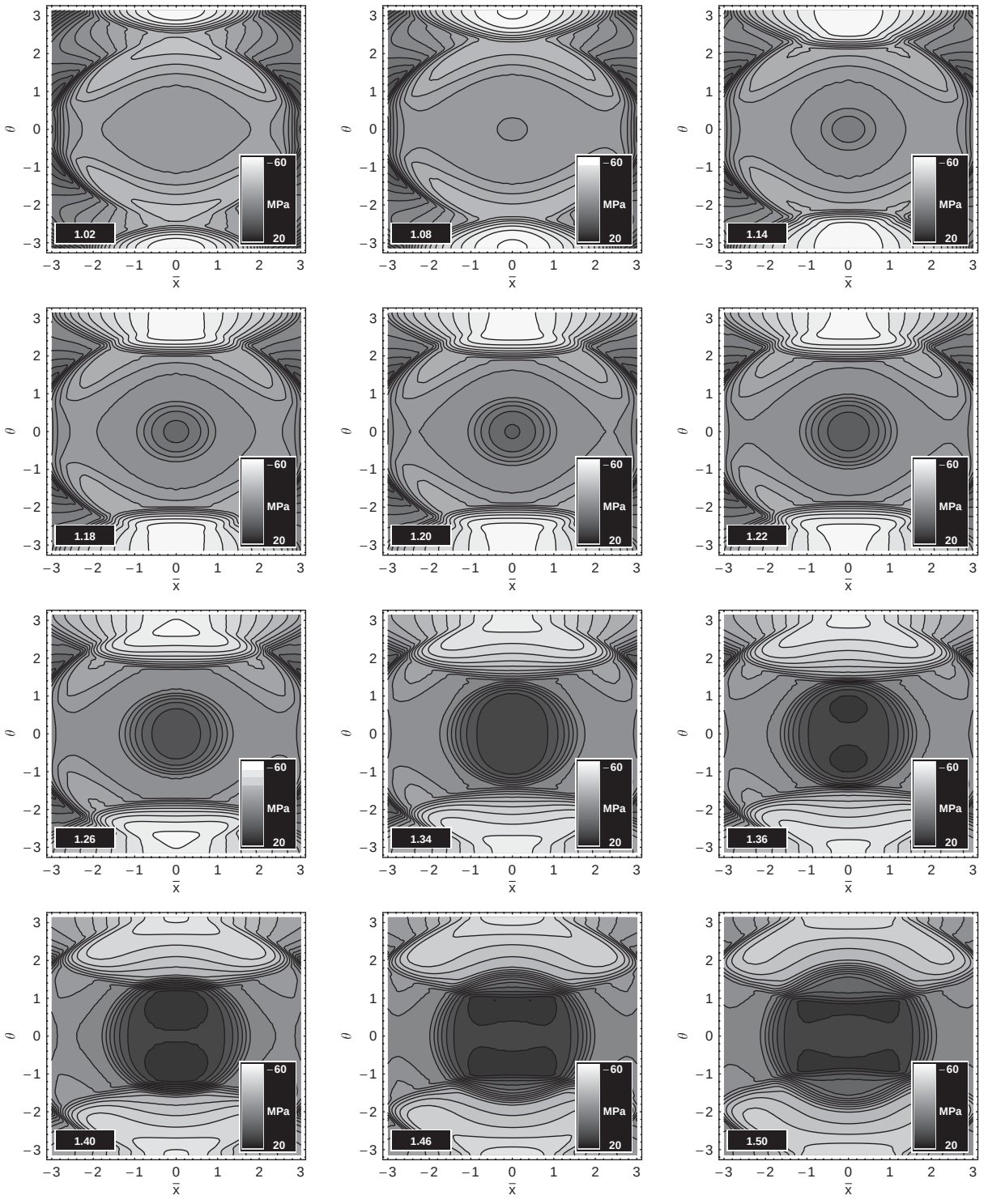

Fig. 15. Dynamics of the transverse stress in the shell with the large-radius core, $t = 1$–1.5.

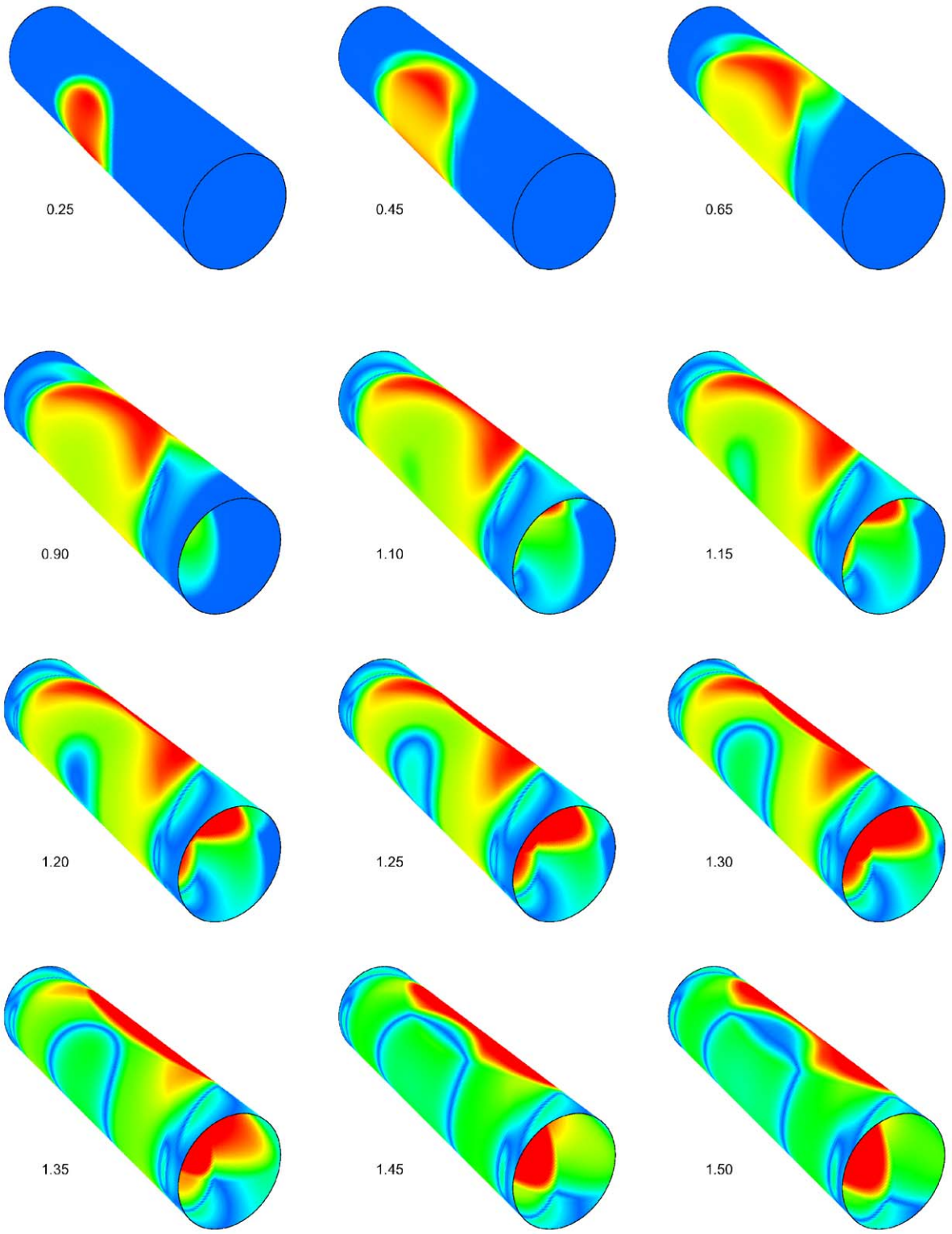

Fig. 16. Three-dimensional dynamics of the transverse stress in the shell with the large-radius core, $t = 0.00$–1.50 (the core is not shown).

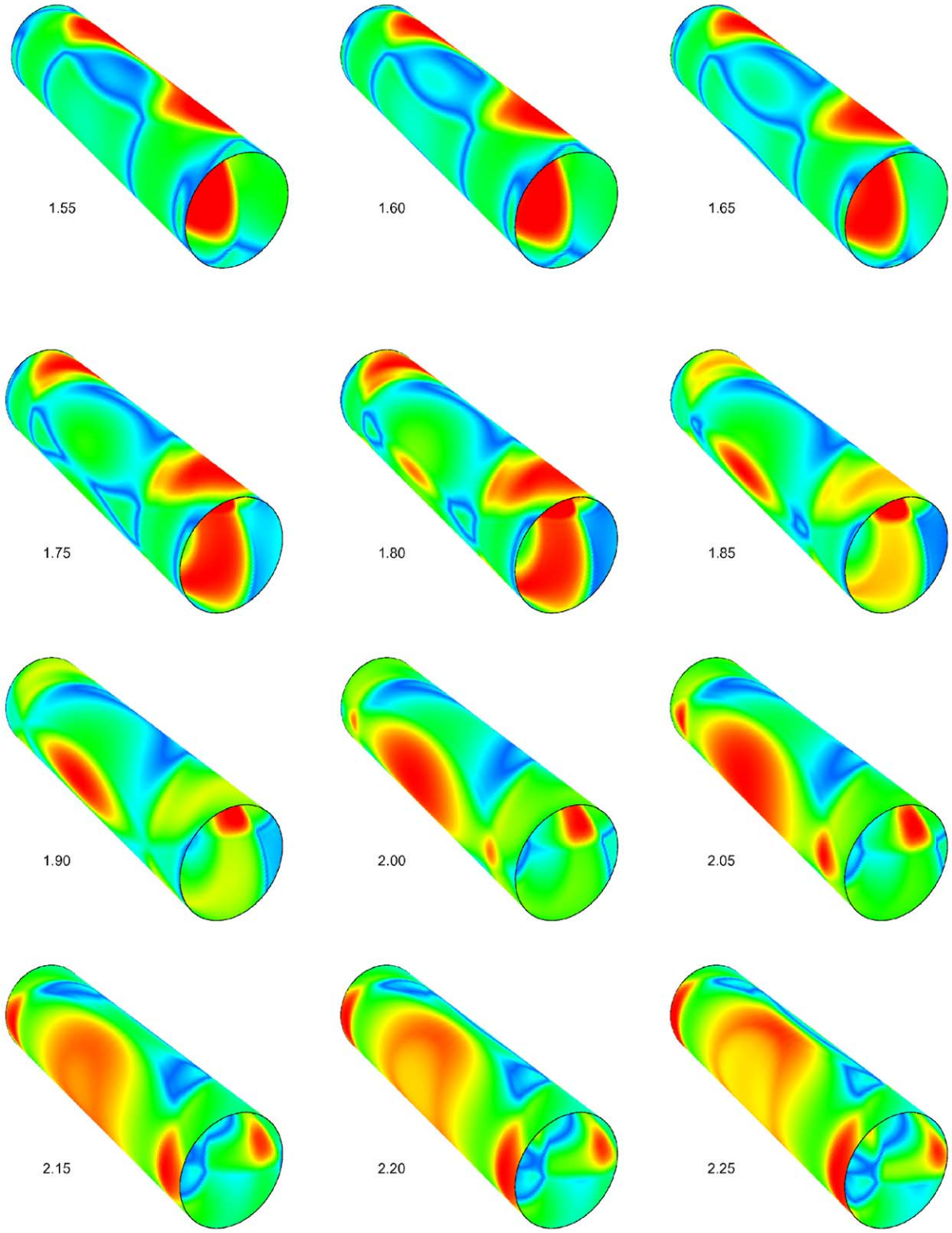

Fig. 17. Three-dimensional dynamics of the transverse stress in the shell with the large-radius core, $t = 1.50$–2.25 (the core is not shown).

From a constructive point of view, the advantages of placing a core inside a shell are, unfortunately, not as obvious as we had hoped. One would be faced with a compromise should one decide to use a rigid core as a constructive measure of safety improvement. Namely, although a large-radius core does provide a considerable reduction of the maximum tensile stress, it also consumes a significant amount of the internal space. However, in some cases this would not be a serious obstacle since often the interior of the core can be efficiently utilized (e.g. it can accommodate equipment, wires etc.). In such cases, a large-radius core appears to be quite a beneficial constructive decision.

In summary, we can conclude that a rigid coaxial core has a significant (and safety-wise beneficial) influence on the stress state of a shell only if the radius of the core exceeds 40% of that of the shell.

Acknowledgements

The author gratefully acknowledges the financial support of the Natural Sciences and Engineering Research Council (NSERC) of Canada, the Killam Trusts at Dalhousie University, and the Faculty of Engineering, Dalhousie University. The advice of Dr Gordon Fenton, Department of Engineering Mathematics, Dalhousie University, regarding some TEX-related issues is appreciated as well.

References

Aanhold, J.E., van Meijer, G.J., Lemmen, P.P.M., 1998. Underwater shock response analysis of a floating vessel. Shock and Vibration 5, 53–59.

Baillard, A., Conoir, J., Decultot, D., Maze, G., Klauson, A., Metsaveer, J., 2000. Acoustic scattering from fluid-loaded stiffened cylindrical shell: analysis using elasticity theory. Journal of the Acoustical Society of America 107, 3208–3216.

Carpenter, R.F., Berger, B.S., 1972. Dynamic response of a seminfinite elastic cylinder containing an acoustic medium. Journal of Applied Mechanics 39, 682–688.

Chambers, G., Sandusky, H., Zerilli, F., Rye, K., Tussing, R., Forbes, J., 2001. Pressure measurements on a deforming surface in response to an underwater explosion in a water-filled aluminum tube. Shock and Vibration 8, 1–7.

Cole, R.H., 1948. Underwater Explosions. Dover Publications, New York.

Drikakis, D., Ofengeim, D., Timofeev, E., Voionovich, P., 1997. Computation of non-stationary shock-wave/cylinder interaction using adaptive-grid methods. Journal of Fluids and Structures 11, 665–691.

Geers, T.L., 1969. Excitation of an elastic cylindrical shell by a transient acoustic wave. Journal of Applied Mechanics 36, 459–469.

Geers, T.L., Zhang, P., 1994a. Doubly asymptotic approximations for submerged structures with internal fluid volumes: formulation. Journal of Applied Mechanics 61, 893–899.

Geers, T.L., Zhang, P., 1994b. Doubly asymptotic approximations for submerged structures with internal fluid volumes: evaluation. Journal of Applied Mechanics 61, 900–906.

Haywood, J.H., 1958. Response of an elastic cylindrical shell to a pressure pulse. Quarterly Journal of Mechanics and Applied Mathematics 11, 129–141.

Huang, H., Wang, Y.F., 1970. Transient interaction of spherical acoustic waves and a cylindrical elastic shell. Journal of Acoustical Society of America 48, 228–235.

Iakovlev, S., 2001. On the numerical inversion of the Laplace transform for the functions $-K_n(s)/(sK'_n(s))$. Report, Dalhousie University.

Iakovlev, S., 2002a. Interaction of a spherical shock wave and a submerged fluid-filled circular cylindrical shell. Journal of Sound and Vibration 225, 615–633.

Iakovlev, S., 2002b. On the singular behavior of the inverse Laplace transforms of the functions $I_n(s)/(sI'_n(s))$. Canadian Mathematical Bulletin 45, 399–416.

Love, A.E.H., 1927. A Treatise on the Mathematical Theory of Elasticity. Cambridge University Press, Cambridge, London.

Mindlin, R.D., Bleich, H.H., 1953. Response of an elastic cylindrical shell to a transverse step shock wave. Journal of Applied Mechanics 20, 189–195.

Ofengeim, D.K., Drikakis, D., 1997. Simulation of blast wave propagation over a cylinder. Shock Waves 7, 305–317.

Touraine, N., Haumesser, L., Decultot, D., Maze, G., Klauson, A., Metsaveer, J., 2000. Analysis of the acoustic scattering at variable incidences from an extra thin cylindrical shell bounded by hemispherical endcaps. Journal of the Acoustical Society of America 108, 2187–2196.

Ugural, A.C., 1981. Stresses in Plates and Shells. McGraw-Hill Book Company, New York.

Wardlaw Jr., A.B., Luton, J.A., 2000. Fluid–structure interaction mechanisms for close-in explosions. Shock and Vibration 7, 265–275.